Journal Pre-proofs

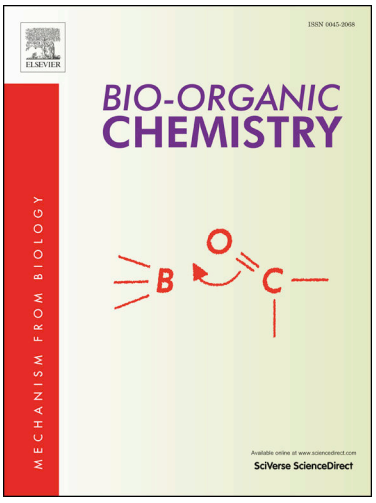

New chalcone-tethered 1,3,5-triazines potentiate the anticancer effect of cisplatin against human lung adenocarcinoma A549 cells by enhancing DNA damage and cell apoptosis

Marwa H. El-Wakil, Sherine N. Khattab, Amira F. El-Yazbi, Nefertiti El-Nikhely, Ahmed Soffar, Hosam H. Khalil

PII: S0045-2068(20)31691-6
DOI: https://doi.org/10.1016/j.bioorg.2020.104393
Reference: YBIOO 104393

To appear in: *Bioorganic Chemistry*

Received Date: 8 April 2020
Revised Date: 6 October 2020
Accepted Date: 15 October 2020

Please cite this article as: M.H. El-Wakil, S.N. Khattab, A.F. El-Yazbi, N. El-Nikhely, A. Soffar, H.H. Khalil, New chalcone-tethered 1,3,5-triazines potentiate the anticancer effect of cisplatin against human lung adenocarcinoma A549 cells by enhancing DNA damage and cell apoptosis, *Bioorganic Chemistry* (2020), doi: https://doi.org/10.1016/j.bioorg.2020.104393

New chalcone-tethered 1,3,5-triazines potentiate the anticancer effect of cisplatin against human lung adenocarcinoma A549 cells by enhancing DNA damage and cell apoptosis

Marwa H. El-Wakil[a], Sherine N. Khattab[b,c] *, Amira F. El-Yazbi[d], Nefertiti El-Nikhely[e], Ahmed Soffar[f], Hosam H. Khalil[b]

[a] Department of Pharmaceutical Chemistry, Faculty of Pharmacy, Alexandria University, Alexandria 21521, Egypt.

[b] Department of Chemistry, Faculty of Science, Alexandria University, Alexandria 21321, Egypt.

[c] Cancer Nanotechnology Research Laboratory (CNRL), Faculty of Pharmacy, Alexandria University, Alexandria 21521, Egypt.

[d] Department of Pharmaceutical Analytical Chemistry, Faculty of Pharmacy, Alexandria University, Alexandria 21521, Egypt.

[e] Department of Biotechnology, Institute of Graduate Studies and Research, Alexandria University, Alexandria 21526, Egypt.

[f] Department of Zoology, Faculty of Science, Alexandria University, Alexandria 21321, Egypt.

Corresponding author

[*]**Sherine N. Khattab:** Department of Chemistry, Faculty of Science, Alexandria University, Alexandria 21321, Egypt. Cancer Nanotechnology Research Laboratory (CNRL), Faculty of Pharmacy, Alexandria University, Alexandria 21521, Egypt. E-mail: sh.n.khattab@gmail.com, sherinekhattab@alexu.edu.eg

Abstract

In the pursuit of new compounds for co-treatment to enhance the anticancer efficacy of cisplatin against lung adenocarcinoma, a series of chalcone-tethered 1,3,5-triazines was designed and synthesized. MTT assay was used to evaluate the anticancer activity of the combinations in which two hybrids **10** and **12** were found to significantly inhibit A549 cancer cells viability and their IC_{50} values were 24.5 and 17 μM, respectively in reference to cisplatin (IC_{50}= 21.5 μM). The combined effect of cisplatin with each of **10** and **12** was analyzed according to Chou-Talalay method against both A549 and normal human fibroblast cells. Mechanistic studies employing MALDI-TOF MS and fluorescence spectroscopy using Evagreen probe inferred that **10** and **12** induced DNA double strand breaks in contrast to cisplatin which induces DNA interstrand cross-links. Also, DNA damage kinetics study demonstrated the difference in the rate of DNA damage induced by both **10** and **12** alone and in combination with cisplatin. Further Annexin V-FITC/propidium iodide dual staining assay provided evidence that **10** and **12** induced apoptosis *via* different pattern to cisplatin and their combination with cisplatin promoted more cells to enter late apoptosis and necrosis. Molecular docking of **10** and **12** in the active pocket of DNA dodecamer displayed their binding

modes with higher number of stable hydrogen bond donor as well as π-H interactions in reference to the original ligand.

Keywords: 1,3,5-Triazinyl chalcones; Cytotoxicity; DNA damage; Molecular Docking; Apoptosis

1. Introduction

Cancer is the second most deadly disease worldwide. The recent advances in cancer research revealed cancer to be a disease characterized by dysfunction in the cell cycle mechanisms with uncontrolled cell proliferation and migration [1]. Recent statistics reported 9.6 million deaths, out of which, lung cancer accounted for nearly 2 million death cases. Lung cancer is now accepted as the most fatal type of malignancies globally, particularly non-small cell lung cancer (NSCLC) constituting 80-90 % of lung cancer cases [2].

Conventional methods for cancer treatment include surgery, radiotherapy and chemotherapy; in which targeted chemotherapy has proven effectiveness in the treatment of various cancer types and its ability to combat cancer cells resistance [3]. Chemotherapeutic agents targeting the DNA constitute one of the most efficient classes of anticancer drugs that possess adequate clinical use and provide enhanced patients' survival rates either used solely or in combination with other drugs [4]. Cisplatin is one of the effective anticancer agents usually directed in the treatment of a number of solid tumors including ovarian, cervical, bladder and NSCLC carcinomas [5–7]. Water solubility and the planar geometry of cisplatin facilitates its incorporation into the DNA double strands forming interstrand cross links [8]. This causes toxic DNA lesions and inhibits DNA strand separation thus halts DNA replication leading to apoptosis. However, cisplatin's clinical use as mono-chemotherapeutic agent suffers limitations due to its nephrotoxicity and adverse side effects towards normal cells [9,10]. Cisplatin's efficacy is diminished by the increasing emergence of resistance that occurs through several ways like decreased drug uptake by cancer cells, drug detoxification by elevated levels of intracellular glutathiones and increased cellular repair of cisplatin-damaged DNA [11]. In an attempt to circumvent the single-use drawbacks of cisplatin, combination therapy with other anticancer drugs has been widely applied for enhancing the anticancer efficacy and limiting cisplatin's therapeutic dose while decreasing the toxic side effects and overcoming the induced drug resistance [12]. This concept of combination therapy, also known as cocktail therapy, is considered the cornerstone in cancer treatment [13]. Some reported successful combinations include synergistic treatment of cisplatin with anticancer drugs as doxorubicin [14], gemcitabine [15] and paclitaxel [16]. Other efficient cisplatin combinations were reported with antitumor compounds of natural origin as triptolide [6], osthole [17], quercetin [18] and curcumin [19]. Moreover, caffeine, although itself does not possess antiproliferative activity, but has shown to enhance the anticancer properties of cisplatin in combination by inhibiting essential proteins involved in the repair of cisplatin-DNA induced damage [20]. The same case was observed with dipyridamole (DPM), a coronary vasodilator, which has proven to

synergistically enhance the cytotoxicity of cisplatin against cisplatin-sensitive human ovarian carcinoma cells by increasing the cellular uptake of cisplatin in a concentration dependent manner [21].

Combination of cisplatin with anticancer small molecule heterocyclic compounds is discussed in the literature [22–25]. From the interesting small molecule heterocyclic scaffolds, 1,3,5-triazines have been intensely studied for their significant wide range of biological activities, especially their anticancer properties [26]. Examples of reported 1,3,5-triazines anticancer drugs include; Altretamine (Hexalen®), **I** [27], Decitabine (Dacogen®), **II** [28], and Azacitidine (Vidaza®), **III** [29] that are employed in the treatment of ovarian cancer, acute myeloid leukemia (AML) and myelodysplastic syndrome (MDS), respectively. Also, there are several anticancer 1,3,5-triazines that have reached phase III clinical trials such as BKM-120, **IV** [30], ZSTK474, **V** [31] and BMCL-200908069-1, **VI** [32] that proved efficacy against different cancer cell lines (**Fig. 1**). The wide interest in the 1,3,5-triazine core has led to synthesis of a large number of derivatives with promising anticancer activities (**Fig. 2, A**) [32–36].

Chalcones, on the other hand, are privileged scaffolds known for their promising diverse biological activities of which the anticancer properties are gaining much attention. The ease of preparation of chalcones make them an appealing synthetic precursor and pharmacologic scaffold [37]. It is believed that chalcones exert their anticancer effect as DNA interactive agents by integration between DNA strands *via* Van der Waal and π-stacking interactions of the chalcone aromatic ring. While the *α,β*-unsaturated carbonyl system provides additional electrostatic hydrogen bond interactions with DNA bases [38]. Furthermore, chalcones are reported to induce apoptosis in cancerous cells [39–41]. As a result, many chalcone based compounds have been reported over the last decade as promising anticancer agents (**Fig. 2,B**) [38,42–47]. Of interest, chalcone-based 1,3,5-triazines have proved to possess valuable anticancer activities [48] but are seldom discussed in the scientific literature. Thus, much attention needs to be paid on the design of new and efficient 1,3,5-triazinyl-chalcone hybrids.

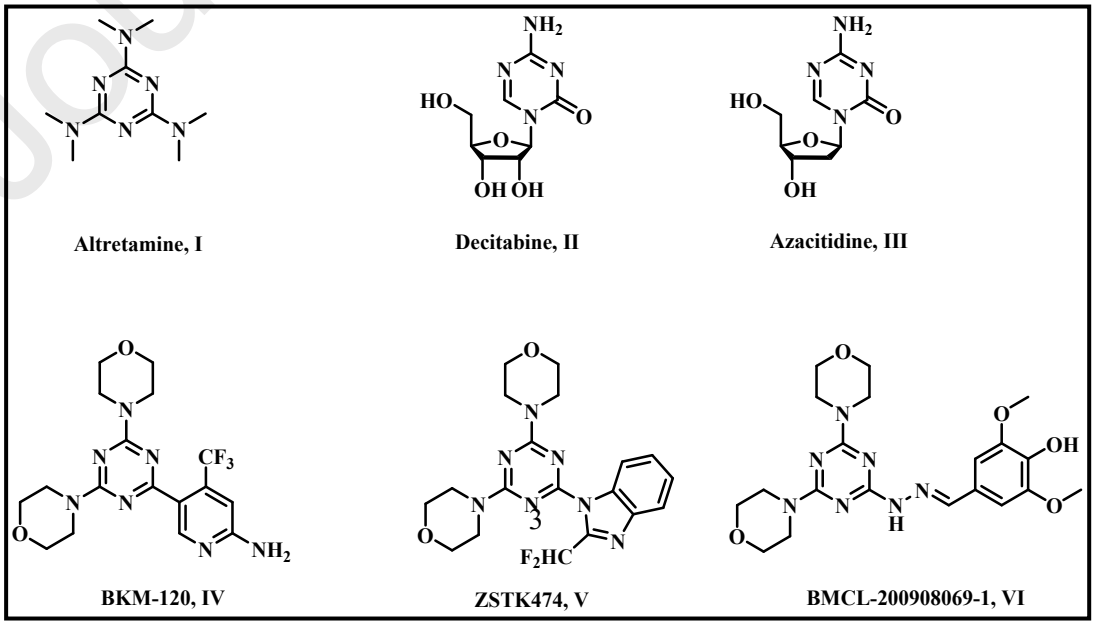

Fig. 1. Anticancer 1,3,5-triazine drugs (**I-III**) and 1,3,5-triazine derivatives in phase III clinical trials(**IV-VI**).

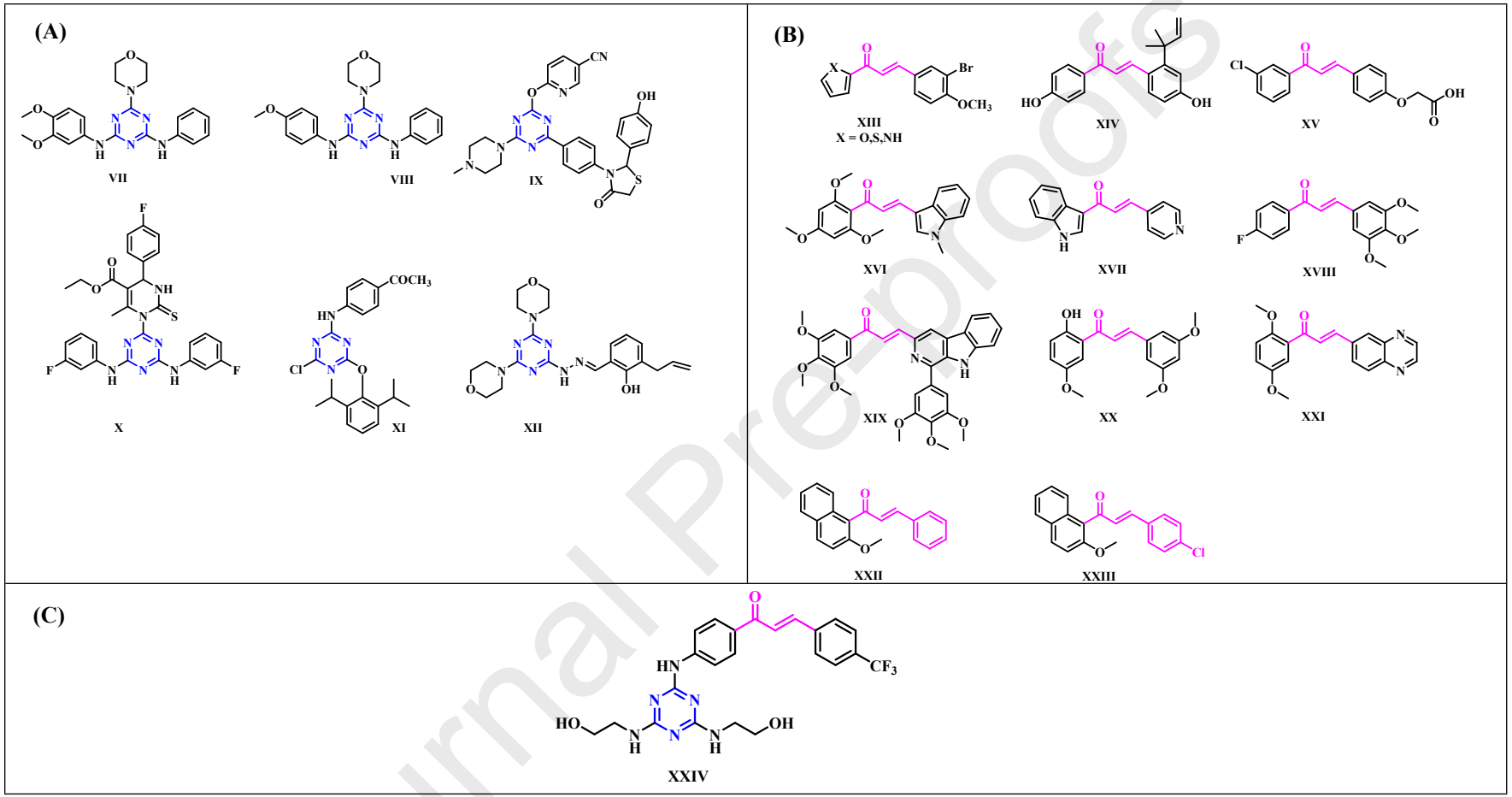

Fig. 2. (A) Some reported anticancer 1,3,5-triazine derivatives, **(B)** Anticancer chalcone-based compounds, **(C)** A reported anticancer 1,3,5-triazinyl chalcone hybrid with GI_{50} = 1.60-15.20 µM in the full panel cell line screening of the US National Cancer Institute (NCI)

2. Rationale and design

Therefore, in continuation of our research efforts in the design and synthesis of novel antitumor agents through DNA binding [49], as well as our chemical interest in the 1,3,5-triazine scaffold [50–52] and prompted by the proven anticancer activities of previously reported 1,3,5-triazines [26,34,35,53,54] and chalcone-based compounds [37,38,40,55,56], we, herein, report the design and synthesis of new chalcone-tethered 1,3,5-triazines. We employed compound **XXII** (**Fig. 2,C**), which is a molecular hybrid between 1,3,5-triazines core and chalcone motif, as our lead compound as it exhibited promising anticancer activities with GI_{50} values in the range 1.60-15.20 µM in the full panel cell line screening of the US National Cancer Institute (NCI) [48]. A structural optimization strategy of the lead **XXIV** was conducted (**Fig. 3**), where the two ethanolamine side chains attached to 1,3,5-triazine ring were substituted to afford four α-amino acid residues namely, glycine, iminodiacetic acid, L-valine and L-phenylalanine. These amino acids are reported to possess promising antitumor activities and found in the structures of a number of anticancer agents [57–59]. While, the trifluoromethyl phenyl ring of the chalcone side chain in **XXIV** was changed to phenyl and *p*-chlorophenyl rings as in chalcones **XXII** and **XXIII** [47]. Primary screening of the antitumor activities of the new compounds is performed against A549 non-small cell lung cancer cell line to select the promising derivatives to be further assessed in combination with cisplatin in order to explore their contributing role in the potential enhancement of the anticancer activity of cisplatin. In addition, molecular recognition studies underlying the possible mechanism of anticancer effect of the active compounds alone and in combination with cisplatin are conducted.

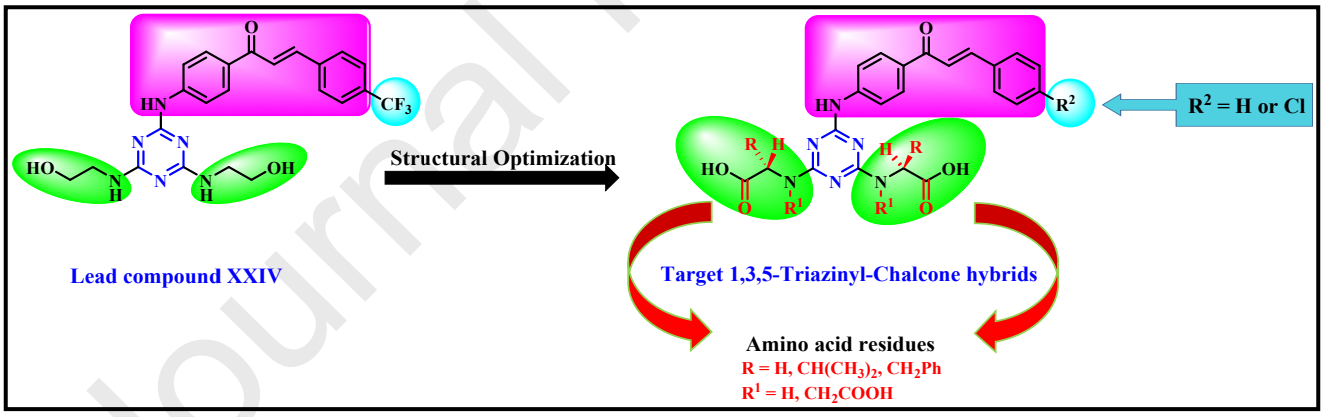

Fig. 3. Design strategy of the target 1,3,5-triazinyl chalcone hybrids through structural optimization of the lead compound **XXIV.**

3. Results and discussion

3.1. Chemistry

The starting compound, 1-(4-((4,6-dichloro-1,3,5-triazin-2-yl)amino)phenyl)ethan-1-one **3** was initially synthesized (**Scheme 1**) by reaction of 2,4,6-trichloro-1,3,5-triazine **1** with 4-aminoacetophenone **2** following the previously reported procedure [48]. Compound **3** was subsequently allowed to react with two equivalent of the appropriate α-amino acid **4** in alkaline medium to produce the corresponding 4-(*N*-(4,6-di-α-aminoacid-1,3,5-triazin-2-yl)amino)acetophenone derivatives **5a-d**. IR spectra of **5a-d** confirmed the presence of carboxylic OH, NH and C=O functionalities. While, ^{1}H NMR spectra of **5a-d** displayed three signals corresponding to the acetophenone moiety, one singlet and two multiplets, at chemical shift ranges 2.47-2.48, 7.72-7.99 and 9.25-9.47 ppm corresponding to methyl, aromatic and N-H protons, respectively. In addition, ^{1}H NMR spectra displayed signals corresponding to methylene or *α*-CH protons of the reacting amino acids at their expected chemical shifts range 3.91-4.60 ppm.

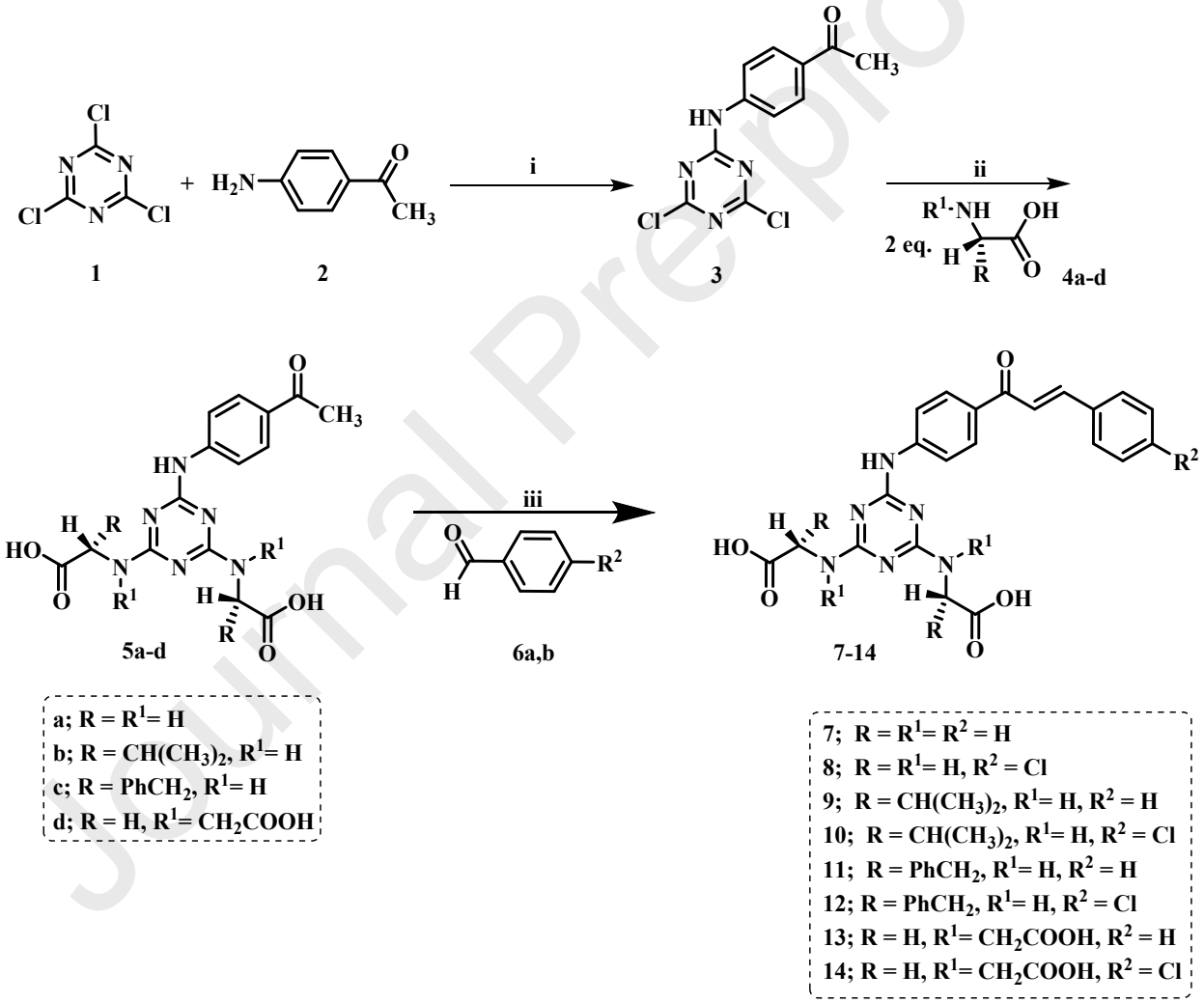

Scheme 1. Synthesis of the new trisubstituted 1,3,5-triazine precursors (**5a-d)** and target 1,3,5-triazinyl chalcone hybrids (**7-14**). **Reagents and conditions:** (**i**) Na_2CO_3, 1,4-dioxane, stir 3 h,

0°C; (**ii**) (a) Na_2CO_3, 1,4-dioxane/water, reflux 12 h, (b) 2N HCl; (**iii**) (a) KOH/ ethanol, stir overnight, rt, (b) 1N HCl.

Furthermore, in ^{13}C-NMR spectra of compounds **5a-d**, methyl, aromatic and carbonyl carbons of acetophenone moiety appeared at chemical shift ranges 26.82-26.86, 116.37-145.78 and 196.85-197.00 ppm, respectively. While, the triazinyl carbons showed three peaks at chemical shift range 164.00-166.41 ppm, indicating that the three carbons are non-equivalent [60,61]. This observation denotes that C_2 and C_4 of the triazine ring possess no plane of symmetry. Taking compound **5c**, as a prototype, two possible conformers (**A** and **B**) could possibly exist (**Fig. 4**), where the HPLC chromatogram of **5c** revealed two peaks in the ratio 93.8%: 6.2%. Therefore, it was of interest to model **5c** using molecular mechanics MM2 calculations. Quantum chemical calculations were carried out with the GAUSSIAN 98 suite of programs. Geometry optimizations were carried out using the DFT level (B3LYP/6-31G**) of theory to assess the relative stability of the different conformers. The calculated relative energies of conformers **A** and **B** of compound **5c** were -1825.99912865 au and -1825.99663867 au, respectively. The computed energies indicated the stability of conformer **A** over conformer **B** by 0.00249 au (1.5625 kcal/mol).

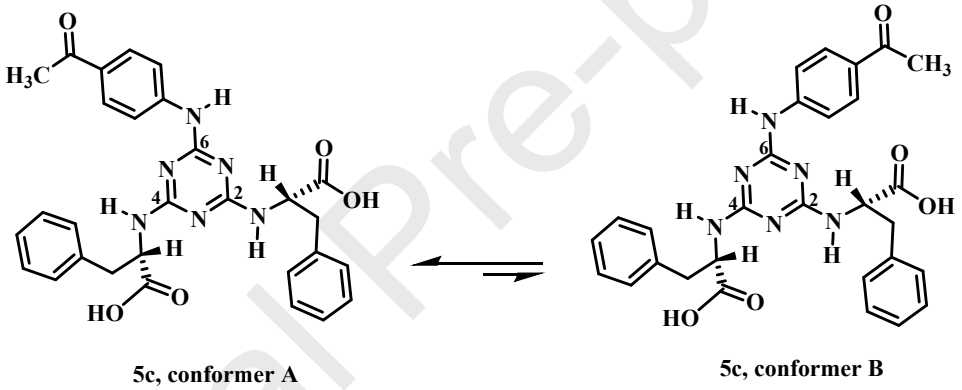

Fig. 4. The expected conformers **A** and **B** of compound **5c**

Claisen-Schmidt condensation of compounds **5a-d** with the selected aromatic aldehydes **6a,b** furnished the corresponding target 1,3,5-triazinyl chalcones **7-14** in moderate yields. Their ^{1}H NMR spectra of compounds **7-14** revealed two doublets attributed to ethylene protons of the *α,β*-unsaturated moiety confirming the complete formation of the chalcone motif. The coupling constant (^3J value) of these ethylene protons was found to be in the range 13.8-15.3 Hz corroborating the *E*-configuration around carbon-carbon double bond [62]. Structural characterization of all new compounds was done applying FT-IR, ^{1}H and ^{13}C NMR as well as elemental analyses. In addition, HPLC analysis was performed for compound **12,** which showed two peaks in the ratio (92.1%: 7.9%), confirming the presence of two conformers of the *E*-isomer. Molecular mechanics MM2 calculations and quantum chemical calculations gave the relative stability of the different conformers. The calculated relative energies of conformers **A** and **B** of

compound **12** were found to be -2554.62199712 au and -2554.62155883 au, respectively (**Fig. 5**). The computed energies indicated the stability of conformer **A** over conformer **B** by 0.00044 au (0.275 kcal/mol).

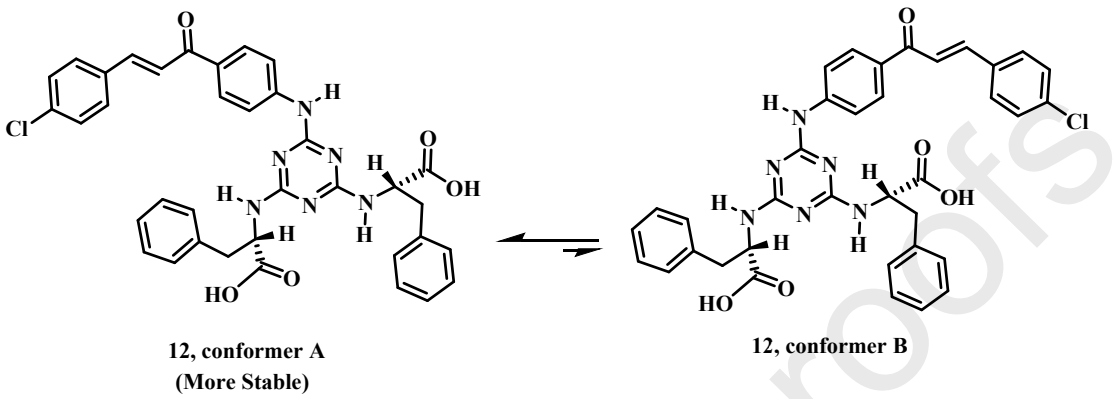

Fig. 5. The two possible conformers of the *E*-isomer of compound **12**.

3.2. Biological evaluation

3.2.1. Antitumor and Cytotoxicity determination using MTT assay

As a preliminary step before assessing the combined effect of cisplatin with the test compounds, antitumor evaluation of **5a-d** and **7-14** expressed as percent cell viability was performed at a single high concentration of 500 µM using MTT tetrazolium dye assay [63] against human NSCLC A549 with DMSO treated cultures as control. Surprisingly, although usually high drug doses are expected to produce more cancer cell killing, the recorded percent cell viability indicated that almost all compounds displayed moderate to weak antitumor activities (**Fig. 6 A**). A possible explanation for this observation could be referenced to the different compensatory mechanisms the cells possess to evade the cellular damage caused by immediate high drug doses, the case which cancer cells consider high intracellular stress condition. Whereas low drug doses would be beneficial in exerting the required antitumor activity [64]. We then continued to examine whether the test compounds influenced the antitumor activity of cisplatin in combination. For each experiment, a concentration of 10 µg/mL of cisplatin was employed to record the control response. Combined application of the test compounds with cisplatin caused a significant reduction in A549 cancer cells viability (< 50% reduction, $p < 0.05$) observed with the target 1,3,5-triazinyl chalcones **10** and **12** compared to their monotherapy indicating potentiated cytotoxicity (**Fig. 6 B**). Thereafter re-evaluation of the antitumor effect of compounds **10** and **12** was performed but using lower doses to calculate the half maximal inhibitory concentration (IC_{50}) of both **10** and **12** which was found to be 24.5 and 17 µM, respectively, in comparison to cisplatin (IC_{50} = 21.5 µM) (**Fig. 7**). The cytotoxicities of **10** and **12** were determined on normal human fibroblast cells isolated from the gingiva and their cytotoxicity (CC_{50}) values were found to be > 30 µM.

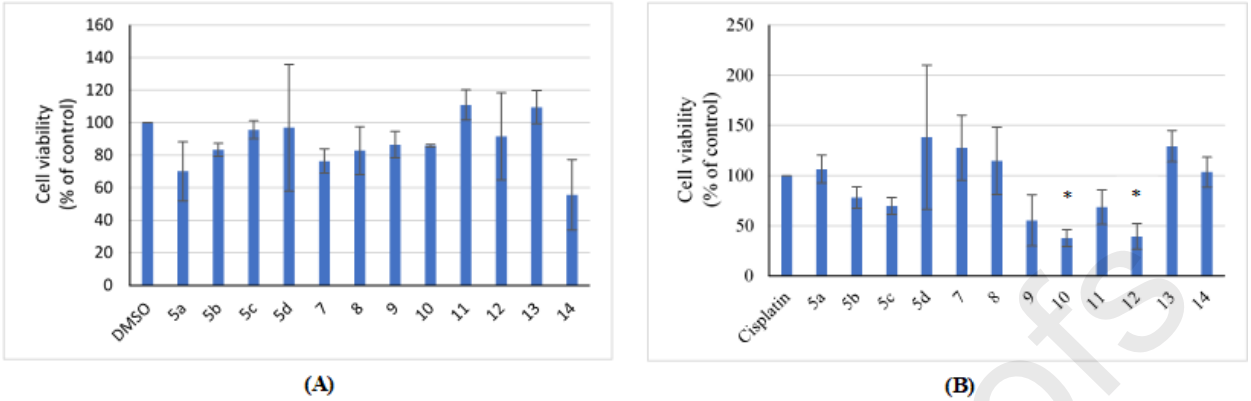

Fig. 6. Bar graph showing the cell viability of A549 cancer cells in response to: **(A)** 500 µM application of compounds **5a-d** and **7-14**. Data are mean ± SE. n = 2, *t*-test. **(B)** 500 µM application of compounds **5a-d** and **7-14** in combination with cisplatin (10 µg/ml). Data are mean ± SE. n = 2, *t*-test, **p* < 0.05.

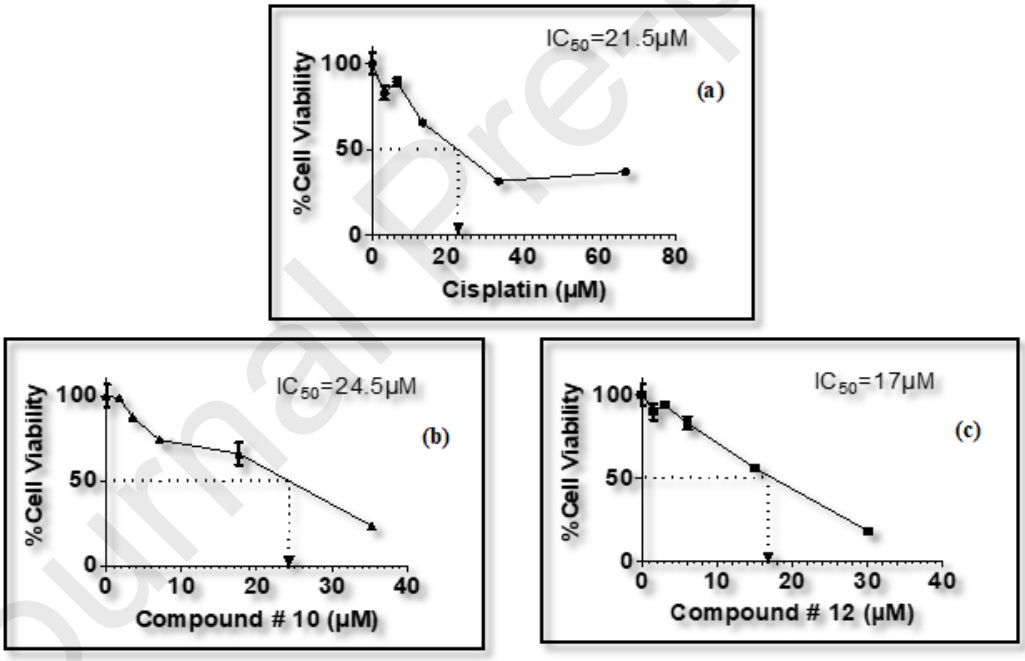

Fig. 7. Sigmoidal dose-response curve-fitting graphs to determine IC_{50} of **(a)** cisplatin (21.5 µM), **(b)** compound **10** (24.5 µM) **(c)** compound **12** (17 µM) against A549 lung adenocarcinoma cancer cells using MTT assay. Cisplatin was used at concentrations of 3.33 µM, 6.66 µM, 13.32 µM, 33.33 µM and 66.6 µM; compound **10** was used at concentrations of 1.76 µM, 3.53 µM, 7.05 µM, 17.6 µM, and 35.27 µM; and compound **12** was used at concentrations of 1.51 µM, 3.02 µM, 6.03 µM, 15.08 µM, and 30.16 µM.

*3.2.2. Combined effect of **10** and **12** on cisplatin's antitumor and cytotoxic activities in A549 cells and normal human fibroblast cells*

In order to investigate how compounds **10** and **12** enhance the antitumor activity of cisplatin against A549 cells either by synergism or additivity, we herein treated A549 cells with constant ratio of equipotent concentrations of cisplatin and **10** or **12**, respectively. Serial dilutions were evaluated to determine the combined effect of cisplatin with **10** and **12**. The combination index (CI) used in this study was determined according to Chou-Talalay method using CompuSyn software[65,66]. CI values close to 1 indicate that the interaction is additive; values less than 1 indicate synergistic interaction; while values greater than 1 represent antagonistic interaction. From the obtained results (**Table 1** and **Figure 8**), the combination of cisplatin at a concentration of 10.75 μM with compound **10** at a concentration of 12.25 μM had CI of 1.035. While the equipotent binary combination of cisplatin (10.75 μM) and compound **12** (8.5 μM) had CI of 1.042. At these concentrations, the affected fraction (fa) was 0.5. The calculated values of CI of both combinations suggest an additive effect. Moreover, the dose reduction index (DRI), which is a measure of the fold reduction of the dose of each compound used in the combination at a given fractional inhibition compared with the doses of each compound alone was calculated. Where, DRI > 1 indicates favorable dose reduction, DRI < 1 indicates unfavorable dose reduction and finally DRI = 1 indicates absence of dose reduction. The equipotent combinations of cisplatin with compounds **10** and **12** at the mentioned assessed concentrations had DRI values in the range 1.79-2.06, implying that approximately two-fold reduction in the doses of cisplatin, **10** and **12** would be favored to attain the required additive effect. In view of these results, both compounds **10** and **12** were further investigated to reveal their underlying mechanism of action by which they potentiate cisplatin's antitumor activity. In order to test whether compounds **10** or **12** have any chemoprotective activity on normal cells, equipotent drug combinations were used to treat normal human fibroblast cells for 48 h before measuring their cytotoxicity. Combination analysis using CompuSyn Software revealed that at fa of 0.5, combining cisplatin with compound **10** had CI of 1.13, whereas combination of cisplatin with compound **12** had CI of 3.8 which suggests an antagonistic effect. This shows that the behavior of both compounds and their combinations is different on cancer cells than normal cells. Further future investigation would be of interest to explore this differential behavior.

Table 1. Data summary of Chou-Talalay method parameters of binary combinations of cisplatin with compounds **10** and **12**, respectively against A549 lung adenocarcinoma cells after 48 h treatment.

Combination treatment	**fa[a]**	**m[b]**	**D_m[c]**	**r[d]**	**CI[e]**	**DRI Cisplatin**	**DRI 10**	**DRI 12**
Cisplatin (10.75 µM) + 10 (12.25 µM)	0.5	0.29248 +/- 0.00172	23.0541	0.99998	1.0354	1.95528	1.91744	
Cisplatin (10.75 µM) + 12 (8.5 µM)	0.52	0.59659 +/- 0.24045	20.6822	0.9275	1.04286	1.79213		2.06244

[a]fa: affected fraction; [b]m: sigmoidicity coefficient; [c]Dm: median effect dose; [d]r: linear correlation coefficient; [e]CI: combination index defines synergistic effect (CI <1), additive effect (CI =1) and antagonistic effect (CI >1).

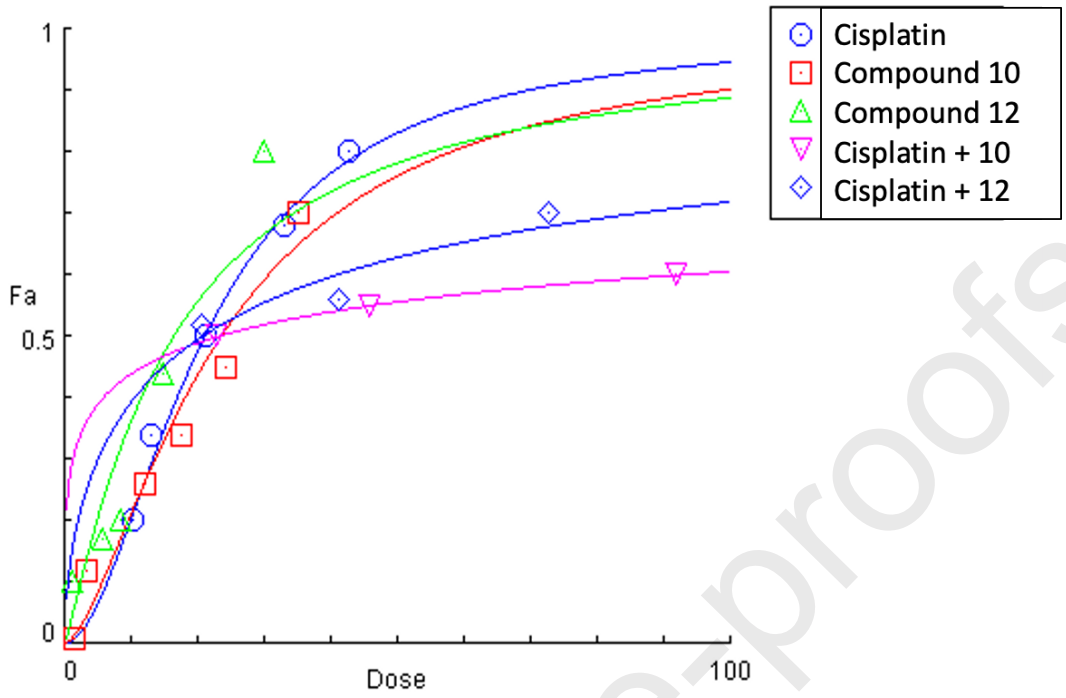

Fig. 8. The dose-effect curves of the single compounds **10**, **12**, cisplatin and their binary combination after 48 h treatment.

*3.2.3. DNA binding studies of **10** and **12***

3.2.3.1. Analysis of DNA damage by MALDI-TOF mass spectrometry

MALDI-TOF MS analysis [67] was studied in reference to the earlier reported MALDI-TOF MS analysis of cisplatin [68]. Initially, the spectrum of a solution of the synthetic double-stranded DNA(dsDNA) sequence, 5'– GTC GCA CGG CAC GGA TAG GTA – 3', 3'–CAG CGT GCC GTG CCT ATC CAT– 5' was recorded alone (**Fig. 9a**) where signals at m/z ~ 6,438 and 3214 are the molecular ions of the intact dsDNA and the single-stranded DNA (ssDNA) forming the dsDNA, respectively with no other significant peaks detected.

Incubation of DNA solution (50 µM) with **10** (500 µM) for 24 h, showed fragments at smaller m/z 727, 1004, 1131 and 1176 (**Fig. 9b**). This indicates that the dsDNA is completely damaged through formation of strand breaks with appearance of molecular ions at shorter m/z values than the intact dsDNA. While solutions of the DNA incubated with (**10+cisplatin)** combination for 24 h, (**Fig. 9c**) similarly displayed complete disappearance of the molecular ion peak of DNA at m/z~6,438 and 3214 with the appearance of the same smaller m/z fragments as the solution of DNA incubated with **10** alone but at higher intensities indicating that more DNA damage has been induced. While after 24 h incubation of DNA solution (50 µM) with **12** (500 µM), the molecular ion peak of the intact DNA at m/z~6,438 and 3214 (**Fig. 9a**) completely disappeared with appearance of fragments

at smaller m/z 655, 825, 1049, 1198, 1322 and 1365 (**Fig. 9d**). Also, upon 24 h incubation of (**12+cisplatin)** combination with DNA (**Fig. 9e**) showed a pattern similar to the solution of DNA with **12** alone. The insets in **Figure 9** focus on the spectra in the region 600–2000 to show the peaks produced upon the reaction of DNA with the test compounds **10** and **12** and that of DNA with (**10+cisplatin)** and **(12+cisplatin)** combination.

It is clear from the spectra in **Figure 9** that no peaks appeared at m/z greater than that of the molecular ion peak of the DNA. This indicates that there is neither covalent modification nor intercalation binding between the studied test compounds and DNA. Instead, the mass spectra after 24 h incubation with both compounds in absence and presence of cisplatin showed the absence of the molecular ion peak of DNA with appearance of other peaks at smaller m/z, hence the formation of smaller DNA fragments, indicating that the DNA predominant damaging effect of both **10** and **12** is likely due to the induced DNA double and single strand breaks. Moreover, the interaction of **10** and **12** with DNA resulted in the formation of peaks with different m/z values. This indicates that the site of interaction of **10** with DNA differs from that of **12**.

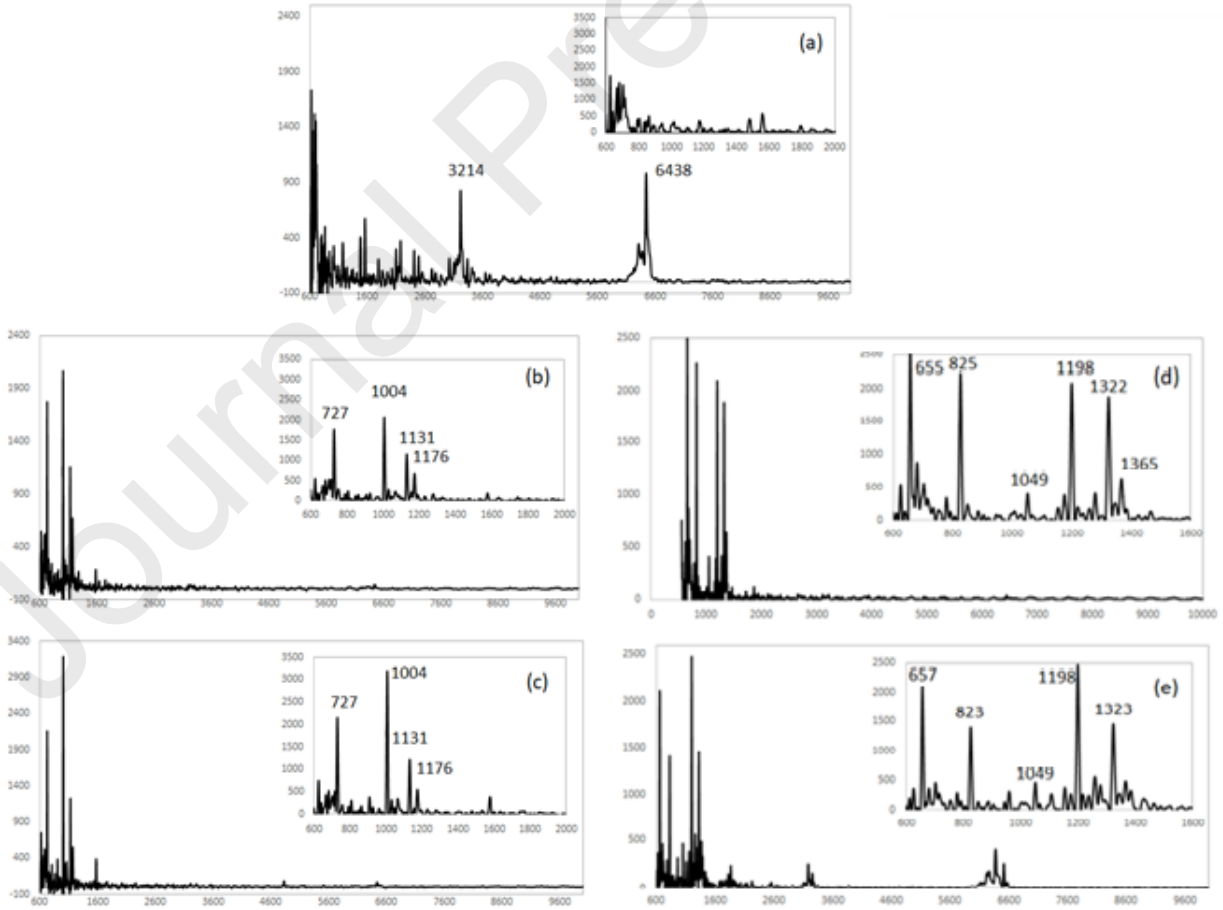

Fig. 9. MALDI-TOF MS after 24 h incubation of **(a)** the synthetic dsDNA (50 μM) sequence alone, where the signals at m/z 6,438 and 3214 are the molecular ion peaks of the DNA sequence, **(b)** in presence of (**10+dsDNA), (c)** in presence of **(10+cisplatin+dsDNA)**, **(d)** in presence of (**12+dsDNA)**, **(e)** in presence of **(12+cisplatin+dsDNA)**. Compounds **10** and **12** were used at 500 μM concentration while cisplatin's concentration was 10 μg/ml.

3.2.3.2. Fluorescence emission studies

Fluorescent DNA probes is another valuable methodology that has been widely used for the detection and quantification of DNA modifications due to binding to small molecules using different probes [69–73]. Of interest, EvaGreen (EG) fluorescent probe shows high sensitivity and selectivity to various DNA modifications [74]. EvaGreen (EG) is formed of two monomers connected to each other with a flexible linker. In presence of dsDNA, the closed loop conformation of EG opens where the two monomers are separated and bind to the dsDNA causing maximum fluorescence. While in case of DNA damage, disruptions to the normal base pairing affects EG binding to the DNA which result in a decrease in EG fluorescence. In this study, EG is selected to detect the DNA structural changes caused by our test compounds **10** and **12** after incubation with the DNA in absence and presence of cisplatin. The kinetics of the interactions detected by the change in EG fluorescence is also investigated fosr dsDNA solution alone and compared with that of solutions of (**10+dsDNA)** and (**12+dsDNA)** mixtures and solutions of (**10+cisplatin+dsDNA)** and **(12+cisplatin+dsDNA)** mixtures (**Fig. 10**). The fluorescence intensity was recorded every minute over a period of 24 h in order to precisely characterize the EG fluorescence changes and the structural changes in the DNA that these mixtures reflect.

EG fluorescence of dsDNA solution alone showed constant maximum fluorescence throughout the 24 h incubation time of the experiment. This indicates that the dsDNA is intact without any disruption in the double helical structure of the DNA. While for solution of (**10+dsDNA)**, the EG fluorescence shows an initial decrease in fluorescence than that of the intact DNA solution. This indicates that immediately after addition of **10** to dsDNA solution, immediate disruption of the DNA structure occurred. Furthermore, the fluorescence intensity decreases gradually and exponentially with increasing incubation time until the fluorescence reaches its minimum intensity after ~200 min incubation. This gradual decrease in fluorescence with time is likey due to the dsDNA damage induced by **10**, which leads to decomplexation of EG with a consequent decrease in fluorescence emission. After 200 min incubation, the fluorescence intensity of the (**10+dsDNA)** mixture remains constant until the end of the 24 h measurements, which indicates that all the EG is completely detached from the damaged DNA and maximum damage has been attained. Moreover, (**10+cisplatin+dsDNA)** mixture revealed an initial decrease in the EG fluorescence even lower than that caused by (**10+dsDNA)** mixture which continues to decrease with increasing the incubation time until it reaches its minimum value after ~100 min incubation after which the fluorescence remains constant at minimum fluorescence till the end of the experiment. Such results indicate that more DNA damage with faster damage kinetics in detected in case of (**10+cisplatin+dsDNA)** mixture (**Fig. 10a**).

Similarly, the fluorescence intensity of (**12+dsDNA)** mixture displayed an initial decrease in the EG fluorescence after immediate addition of **12** to DNA which further decreased gradually and exponentially with incubation time until reaching its minimum after~100 min incubation, after which it remained constant at minimum fluorescence until the end of the 24 h measurements . Also, (**12+cisplatin+dsDNA)** mixture caused an initial decrease in EG fluorescence showing faster damage kinetics than (**12+dsDNA)** mixture (**Fig. 10b**).

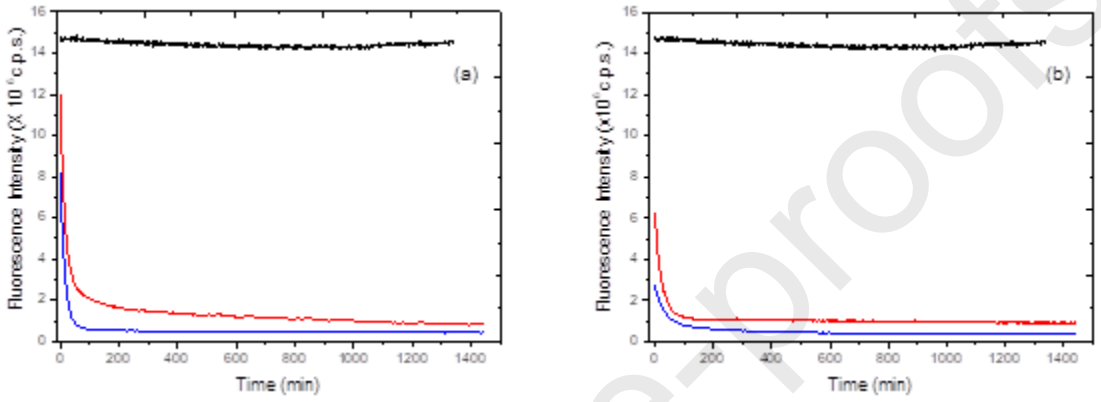

Fig. 10. EG fluorescence intensity in c.p.s. (counts per second) of the dsDNA-EG complex as a function of incubation time with **(a)** compound **10** (10 μM) **(b)** compound **12** (10 μM)**,** in presence (blue line) and absence (red line) of cisplatin (5 μM). EG fluorescence of the DNA (0.2 μM) alone (black line) is also shown. The excitation wavelength is 490 nm and the emission wavelength is 530 nm.

In order to compare the kinetics of the decrease in EG fluorescence induced by the two test compounds **10** and **12** in presence and absence of cisplatin, the fluorescence plots (**Fig. 10**) were fit to a single exponential function: $IF = IF0 + Ae - t/\tau$ where, I_F is the fluorescence intensity at time t, I_{F0} is the fluorescence intensity at time 0, A is the amplitude, and $e^{-t/\tau}$ is the exponential decay with τ representing the damage constant. This fit allows us to determine the rate of decrease in fluorescence intensity with incubation time. All exponential fits to the rate of DNA damage induced by the studied compounds are presented in **Table 2**. The faster the decrease in the fluorescence intensity with time, the smaller the damage constants (τ) obtained from the exponential fits and the faster the rate of DNA damage induced by the test compound. Results shown in **Figure 10** and **Table 2** indicate that both **10** and **12** have different damage kinetics. Also, the combination of compounds **10** and **12** with cisplatin caused a pronounced decrease in the damage constant, reflecting the greater rate of DNA induced damage. Results obtained from the EG fluorescence emission spectrophotometry perfectly matches those obtained from the MALDI-TOF experiment and confirms that both **10** and **12** have different modes of DNA interactions. In both investigations, the combination of **10** and **12** with cisplatin show enhanced DNA damaging effects which would interpret their observed potentiated cytotoxicity.

Table 2. EvaGreen fluorescence curve fitting parameters showing the effect of compounds **10** and **12** at 10 μM concentration each on the damage induced in the dsDNA sequence in absence and presence of cisplatin (5 μM).

Damage kinetics parameters	**10+dsDNA**	**10+cisplatin+dsDNA**	**12+dsDNA**	**12+cisplatin+dsDNA**
$I_{F,0}$ (c.p.s.)	$1.18 \pm 0.08 \times 10^6$	$4.78 \pm 0.01 \times 10^5$	$9.98 \pm 0.02 \times 10^5$	$4.54 \pm 0.08 \times 10^6$
A (c.p.s.)	$9.5 \pm 0.1 \times 10^6$	$7.7 \pm 0.02 \times 10^6$	$4.86 \pm 0.02 \times 10^6$	$3.93 \pm 0.13 \times 10^6$
τ (min)	19.91 ± 0.32	11.68 ± 0.04	17.54 ± 0.13	15.04 ± 0.72

3.2.3.3. Probing DNA damage using calf thymus DNA

The potency of our studied compounds **10** and **12** regarding the induction of DNA damage was assessed by examining their effect on natural calf thymus DNA (ctDNA) in absence and presence of cisplatin. Different concentrations (0 – 100 μM) of each compound was mixed separately with ctDNA. The fluorescence of each concentration was measured after adding EG. **Figure 11** presents the fluorescence intensity versus the concentration of each compound. At zero concentration of each compound, maximum fluorescence was recorded indicating that the ctDNA is intact and undamaged. Increasing the compounds concentration led to a gradual decrease in the fluorescence intensity as more DNA damage is induced until reaching a concentration in the range of 5 - 10 μM of each of the studied compounds alone and with cisplatin (10 μM) after which no further decrease in fluorescence occurred indicating maximum damage attained. The quantification parameters of the DNA damage (**Table 3**) induced by the studied compounds alone and in presence of cisplatin were obtained from data of **Figure 11** where the insets represent the linear region in each plot. The linearity was studied to estimate the minimum concentration of each compound that caused DNA damage (LOD). LOD values obtained for the four mixtures indicated that combination of cisplatin with **10** and **12** showed better results than each test compound alone, where a concentration as low as 10 nM of compound **10** and 37 nM of compound **12** in presence of cisplatin is enough to cause detectable damage to the ctDNA.

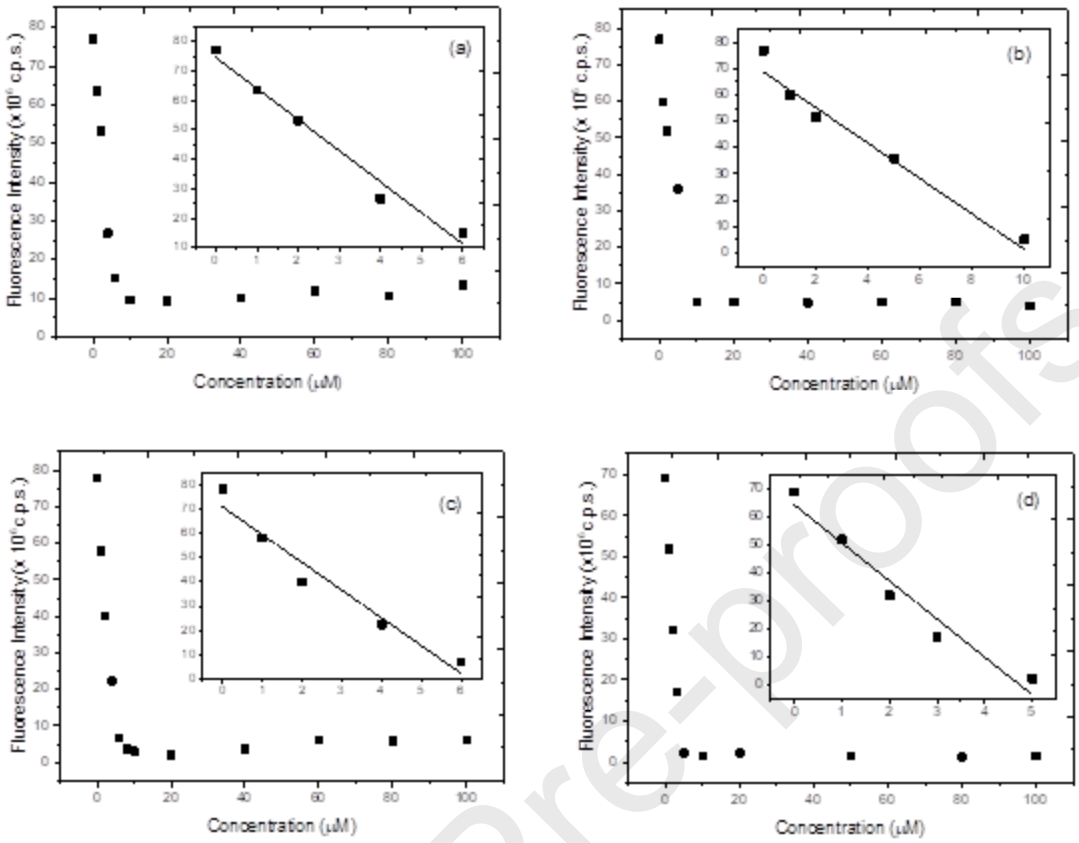

Fig. 11. Calibration curves of DNA damage formed upon incubation of ctDNA (0.01 μM) as a function of **(a)** the concentration of compound **10** alone **(b)** 10 μM of cisplatin in presence of **10** **(c)** compound **12** alone **(d)** 10 μM of cisplatin in presence of **12**. The insets show the fit to the linear portions of the calibration curves.

Table 3: Analytical parameters for the fluorescence measurements of the studied compounds **10** and **12** with ctDNA mixtures in absence and presence of 10 μM cisplatin.

Parameter	**10+dsDNA**	**10+Cisplatin +dsDNA**	**12+dsDNA**	**12+Cisplatin +dsDNA**
Linear dynamic range (μM)	1.0 – 6.0	1.0 - 10.0	1.0 - 6.0	1.0 – 5.0
Correlation coefficient (r)	0.991	0.998	0.976	0.977
Intercept (a)	7.45×10^7	6.86×10^7	7.07×10^7	6.43×10^7
Slope (b)	-1.06×10^7	-6.73×10^7	-1.14×10^7	-1.85×10^7
LOD[a] (μM)	0.064	0.010	0.059	0.037
LOQ[b] (μM)	0.213	0.034	0.198	0.122

[a] LOD: Limit of detection, [b]LOQ: Limit of quantitation.

3.2.4. DNA binding mode analysis

Molecular docking simulation of compounds **10** and **12** were carried out using Molecular Orbital Environment [75] (MOE 2016.08.02) in order to gain perception about their potential binding mode to the DNA and to validate the results obtained from the DNA binding studies. Both compounds were docked in the DNA dodecamer obtained from the protein data bank (PDB code: 2DND) with respect to the original ligand, distamycin. The preferred binding modes based on the structures with the least binding energies were further explored for their 2D and 3D interactions (**Fig. 12**). The calculated free energy of binding (ΔG) for **10** and **12** were found to be -10.17 and -10.02 Kcal/ mol, respectively in comparison to the original ligand (ΔG -8.30 Kcal/mol). The original ligand showed hydrogen bond (H-bond) donor interaction concerning NH and thymidine base DT:B18 and π-H interaction between pyrrole ring and DT:B20 (**Fig. 12a**).

As seen from the figures of interactions, compounds **10** and **12** bind to DNA double strands, in which **10** (**Fig. 12b**) showed key H-bond interaction between thymidine base DT:B20 and OH group of one valine carboxylic side chain. Also, it displayed additional H-bond donor interactions involving thymidine base pairs DT:A8 and DT:A9 with OH group of the other valine carboxylic side chain and anilino N, respectively. Furthermore, two π-H interactions were observed; one involving 4-chlorophenyl ring of chalcone moiety with DT:A7 and the other is between 1,3,5-triazine core and DT:A9. Also, compound **12** (**Fig. 12c**) revealed key H-bond donor interaction with DNA dodecamer involving DT:B20 and OH of one phenylalanine carboxylic group. Another H-bond donor interaction was detected involving DT:A8 and NH of the second phenylalanine moiety. Again, two π-H interactions were seen, one between 4-chlorophenyl ring of chalcone moiety and DT:21 while the other involved 1,3,5-triazine ring and DT:A8.

It could be concluded from the docking simulation study the following points:

a) Both 4-chlorophenyl of chalcone moiety and 1,3,5-triazine rings are responsible for the DNA binding properties of **10** and **12** through strong π-H interactions. This confirms the importance of our design of new chalcone based 1,3,5-triazine hybrids.
b) Valine and phenylalanine residues in **10** and **12**, respectively, provide two H-bond donor interactions necessary for accurate DNA binding in comparison to the original ligand which demonstrates only one H-bond donor interaction with DNA dodecamer.
c) **10** and **12** interact with both DNA strands. This is in consistence with DNA binding studies which confirms occurrence of DNA double strand breaks as revealed from results of the MALDI-TOF and fluorescence spectrometry experiments.
d) Both **10** and **12** selectively bind to thymidine base pairs similar to the original ligand. Also, they interact with different thymidine base pairs, thus having different binding modes to the DNA and emphasizes the obtained results of their different DNA damage kinetics study results as well.

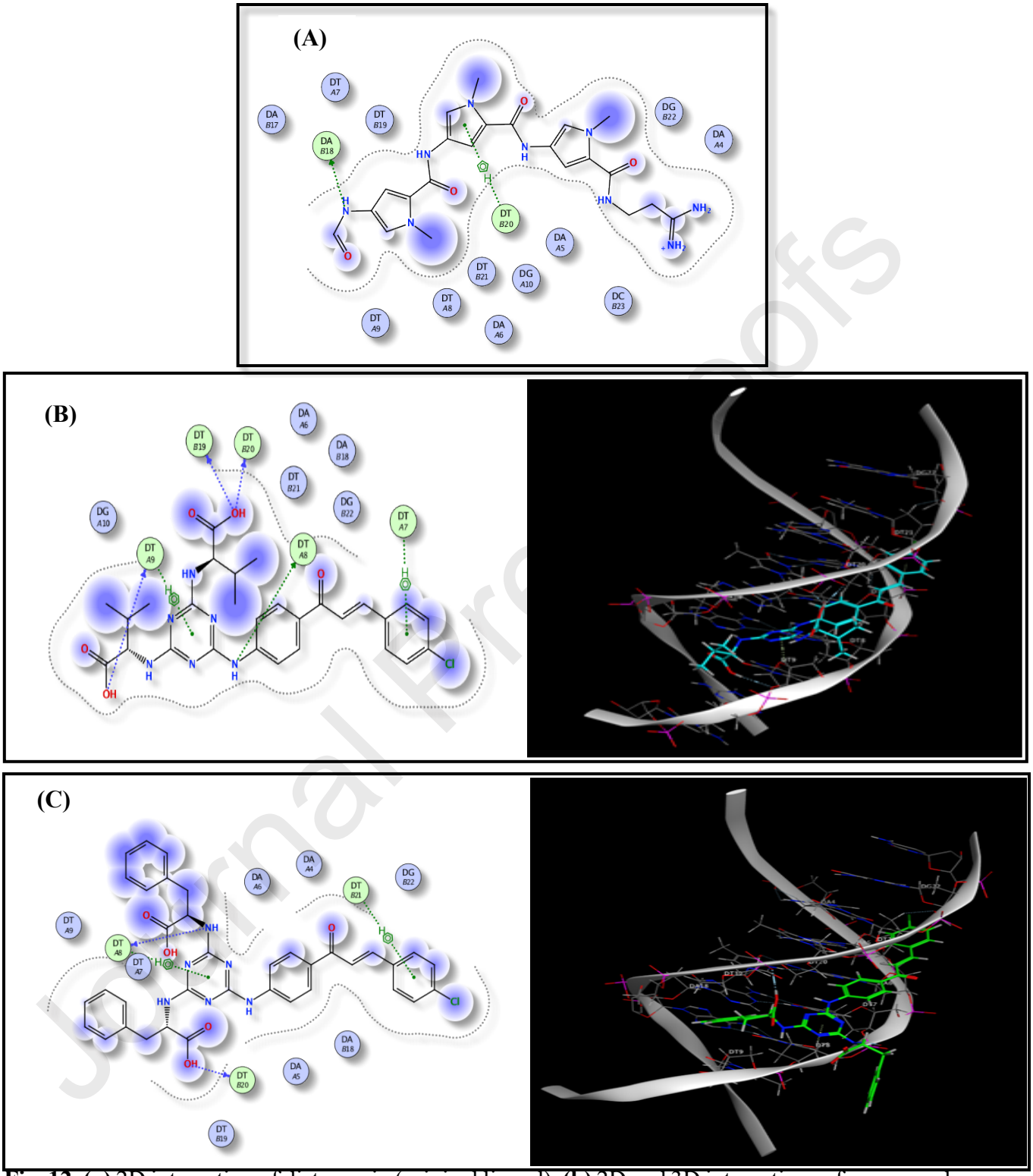

Fig. 12. (a) 2D interaction of distamycin (original ligand), **(b)** 2D and 3D interactions of compound **10** (cyan color) **(C)** 2D and 3D interactions of compound **12** (green color) all showing the key binding interactions with DNA bases of DNA dodecamer (grey ribbon) (PDB code: 2DND).

3.2.5. Detection of Apoptosis using Annexin V-FITC/Propidium iodide (Annexin V-FITC/ PI) double staining

The anticancer effect of DNA binding agents relies on the induction of apoptosis as a consequence of DNA damage [76]. Therefore, the apoptotic changes of cisplatin, **10** and **12** alone and combined with cisplatin were assessed in A549 cancer cells using Annexin V-FITC/ PI double staining method followed by flow cytometry measurement [77] in order to give qualitative insights about the mechanism by which each compound and its combination with cisplatin affect apoptosis. Flow cytometry technique differentiates between viable cells, early apoptotic cells, late apoptotic cells and necrotic cells (**Fig. 13**). Cancer cells were treated with cisplatin (21.5 μM), compound **10** (24.5 μM) and **12** (17 μM) for 24 h and then stained by Annexin V-FITC followed by staining with propidium iodide. As depicted in **Figure 14**, it was observed that cisplatin mainly induced around 21.96 % of the cells to enter early apoptosis while 2.69 % of the cells were in late apoptosis with total number of dead cells reaching 42.08%. Whereas, compounds **10** and **12** induced early apoptosis only in 2.47% and 1.90 % of the cells, respectively, with less number of total dead cells in comparison to cisplatin. When cells were treated with a combination of cisplatin (21.5 μM) and compound **10** (24.5 μM) or **12** (17 μM), more cells were detected in late apoptosis and necrosis in comparison to cisplatin. Such results indicate that compounds **10** and **12** have a mechanism of action different from cisplatin to affect cell viability. This emphasizes the later results obtained from the DNA binding studies and molecular docking simulations, where compounds **10** and **12** probably take time to cause DNA double strand breaks thus mainly affect late apoptosis and necrosis. On the other hand, cisplatin rapidly intercalates the DNA strands thus forcing more cells into early apoptosis. This experiment provides evidence that combination of cisplatin with both compounds **10** and **12** resulted in potentiation of the anticancer activity of cisplatin with total number of dead cells reaching 43.68 % and 42.25 %, respectively. Further detailed concentration-dependent and time-dependent investigations would be of interest in future work.

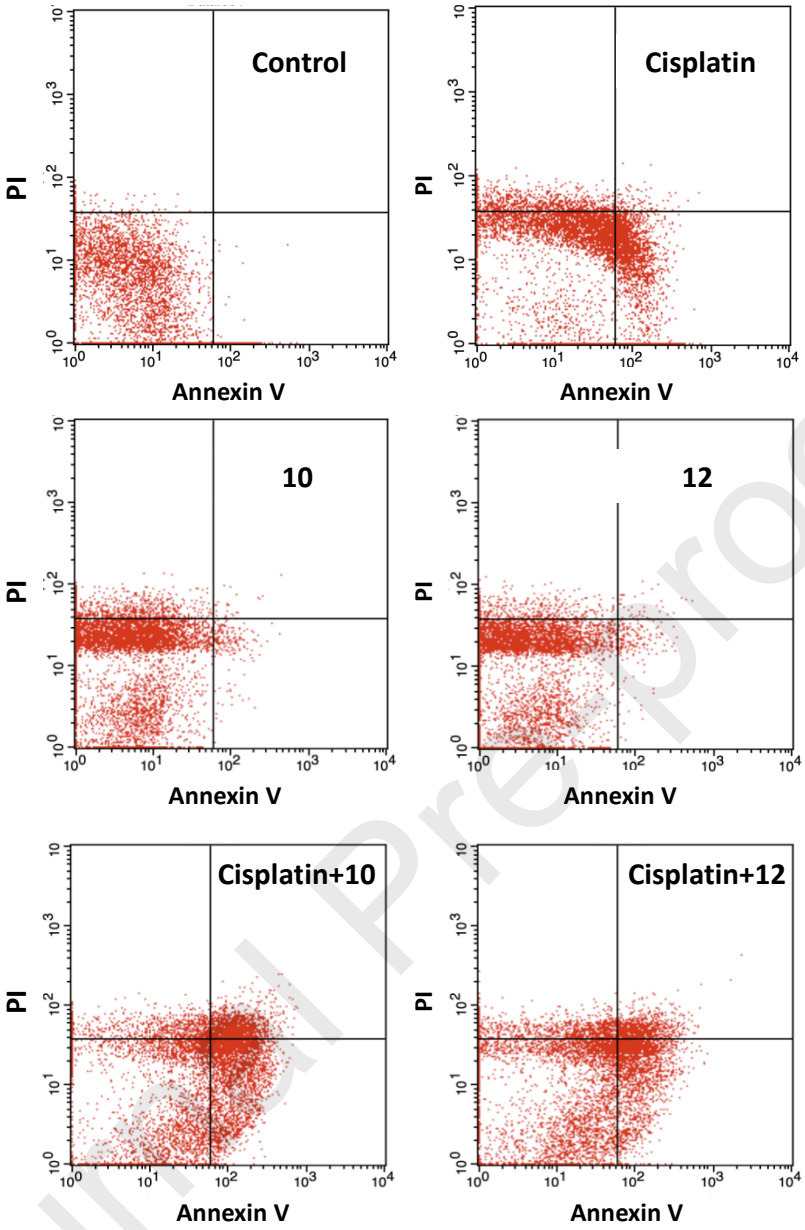

Fig. 13. Dot plot representation of apoptosis analysis by flow cytometric analysis using Annexin V-FITC/propidium iodide dual staining technique for cisplatin (21.5 μM), compound **10** (24.5 μM**)**, compound **12** (17 μM**)** and their combination with cisplatin. Each histogram is divided into 4 quadrants; upper left quadrant represents necrotic cells, upper right quadrant shows late apoptotic cells, lower left quadrant demonstrates viable cells, and lower right quadrant displays early apoptotic cells. Data represented are the mean values ± SEM for three independent experiments. Statistical significance was assess by two-way ANOVA test.

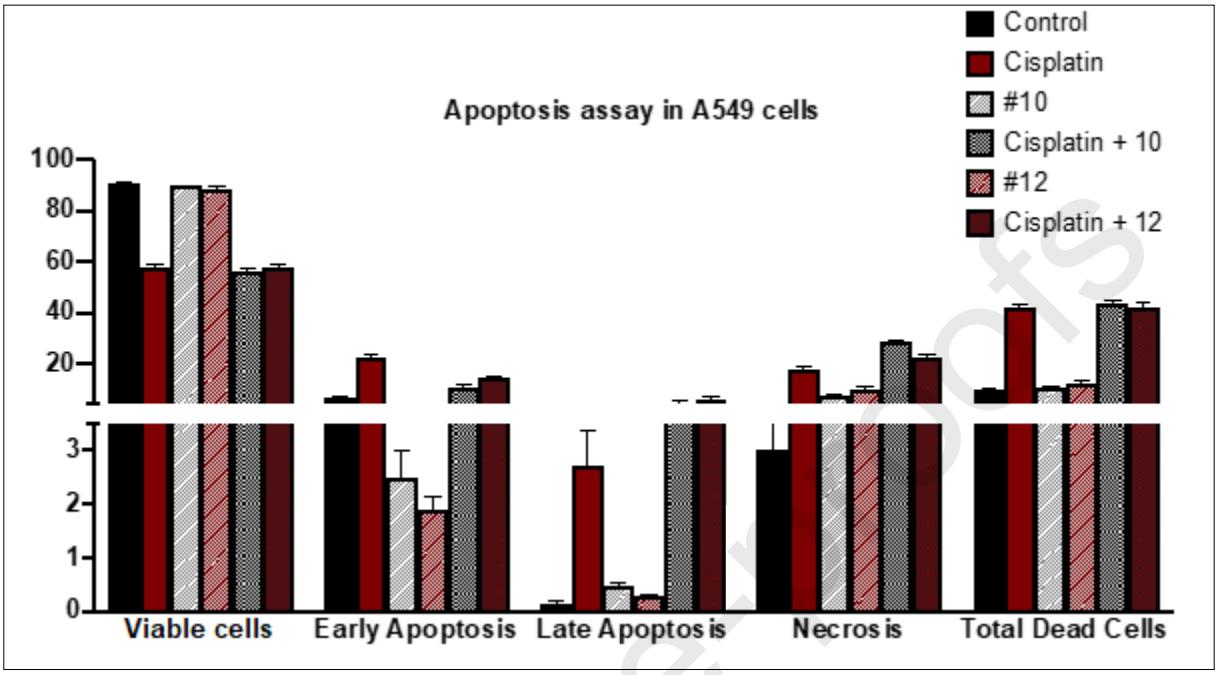

Fig. 14. Graphical representation of the effect of cisplatin (21.5 μM), compound **10** (24.5 μM), compound **12** (17 μM) and their combination with cisplatin when incubated 24 h with A549 cancer cells on apoptotic stages and necrosis using Annexin V-FITC/PI assay by flow cytometry. Data are presented as mean values ± SEM for three independent experiments. Statistical significance was assessed by two-way ANOVA test.

4. Conclusion

In summary, we have synthesized a new series of chalcone-tethered 1,3,5-triazines by structural optimization of a previously reported lead compound. The new hybrids were characterized by IR, ^{1}H and ^{13}C NMR besides elemental analyses. Anticancer activity of these compounds were evaluated in A549 lung cancer cells using MTT assay in absence and presence of cisplatin in order to detect the potential hybrids that would improve the anticancer effect of cisplatin. Amongst all the synthesized derivatives, compounds **10** and **12** displayed significant reduction in cell viability in combination with cisplatin. Additional combinational analyses according to Chou-Talalay method were performed, in which cisplatin combined with either **10** or **12** had CI =1 indicating additive antitumor effect, while the combinations displayed CI >1 against normal human fibroblasts suggesting antagonistic effect. Furthermore, compounds **10** and **12** were subjected to a

detailed mechanistic study to reveal their mechanism of antitumor activity. DNA binding studies were conducted employing MALDI-TOF MS and fluorescence spectroscopy where the results showed that both **10** and **12** caused DNA double strand breaks more prominent in combination with cisplatin. Besides, the damage kinetics of **10** and **12** proved that they both have different mode of DNA interactions. These observations were further confirmed by analyzing their binding mode with DNA dodecamer in a molecular docking simulation to understand their preferred orientation with DNA. Finally, apoptosis induction assay of **10** and **12** in combination with cisplatin emphasized that they possess a mechanism of action different from cisplatin to affect cell viability. Taking into consideration the above-mentioned findings, this study signifies the exciting impact of the anticancer potency of the newly synthesized 1,3,5-triazinyl chalcones **10** and **12** as adjuvant agents to enhance the anticancer activity of cisplatin in human lung adenocarcinoma.

5. Experimental section

5.1. Chemistry

5.1.1. Materials and measurements

All solvents and reagents were purchased from Sigma-Aldrich without further purification. Reaction progress was monitored using thin layer chromatography (TLC) using aluminum-backed Merck Silica Gel 60 F-254 plates applying ethyl acetate/ n-hexane (1:3) as eluent, where spots were visualized by a Spectroline UV Lamp at 254 nm or I_2 vapor. An Agilent 1260 Infinity HPLC system was used. The HPLC analysis was carried out with an Agilent Zorbax Eclipse XDB C_{18} reversed-phase column (250×4.6 mm, 5 µm particle size) maintained at room temperature. Melting points were measured in open capillary tubes using a MEL-Temp II melting point apparatus and were uncorrected. Perkin-Elmer 1600 series Fourier transform instrument was used in recording Infrared (IR) spectra in ύ, cm^{-1} using KBr discs. ^1H and ^{13}C NMR spectra were recorded on JEOL 500 MHz spectrometer at ambient temperature operating at 500 and 125 MHz, respectively. Chemical shifts were reported in parts per million (ppm) and are referenced relative to DMSO at δ 2.50 ppm for DMSO-d_6 using TMS as internal standard. Types of signals were designated by one of these letter symbols: s = singlet, br.s = broad singlet and m = multiplet. Elemental analyses were performed on a Perkin-Elmer 2400 elemental analyzer, and values obtained were found to be within ±0.4 % of the theoretical ones.

*5.1.1.1. General procedure for synthesis of precursors **5a-d***

To an ice-cold mixture of 2,4,6-trichloro-1,3,5-triazine **1** (1.84 g, 10 mmol) and Na_2CO_3 (1.06 g, 10 mmol) in dioxane (20 mL), a solution of 4-aminoacetophenone **2** (1.35 g, 10 mmol) in dioxane (20 mL), was added drop wise with stirring for 3 h. Subsequently, the selected *α*-amino acid **4a-d** (25 mmol) in Na_2CO_3 solution (5.3 g, 20 mL) was added and the reaction mixture was heated under reflux for 12 h. The reaction mixture was then cooled to room temperature and neutralized with 2N HCl. The formed precipitate was filtered off, washed with water, dried and recrystallized from ethanol to give the corresponding 1,3,5-triazinyl-acetophenone derivatives **5a-d**.

*5.1.1.1.1. 2,2'-{[6-(4-Acetylanilino)-1,3,5-triazine-2,4-diyl]diazanediyl}diacetic acid (**5a**).* White solid, yield: 77.2 %; m .p. 232-234°C; IR (KBr, cm^{-1}): 3600-2800 (br, OH, acid), 3383 (NH), 1703, 1641 (C=O); ^{1}H-NMR (500 MHz, DMSO-d_6): δ 2.47 (s, 3H, $COCH_3$), 3.91 (s, 4H, 2 *α*-CH_2), 7.19-7.33 (m, 2H, 2NH, D_2O exchangeable), 7.82-7.93 (m, 4H, Ar-H), 9.42-9.47 (m, 1H, NH, D_2O exchangeable); ^{13}C-NMR (125 MHz, DMSO-d_6): δ 26.82, 42.46, 42.71, 116.39, 118.77, 129.68, 130.29, 145.78, 164.38, 166.12, 166.41, 172.61, 172.68, 197.00. Anal. calcd. for $C_{15}H_{16}N_6O_5$ (%): C, 50.00; H, 4.48; N, 23.32. Found: C, 49.85; H, 4.61; N, 23.44.

*5.1.1.1.2. 2,2'-{[6-(4-Acetylanilino)-1,3,5-triazine-2,4-diyl]diazanediyl}bis(3-methylbutanoic acid) (**5b**).* White solid, yield: 55.9 % ; m.p. 202-205°C; IR (KBr, cm^{-1}): 3650-3000 (br, OH, acid), 3410 (NH), 1722, 1661 (C=O); ^{1}H-NMR (500 MHz, DMSO-d_6): δ 0.93 (s, 12H, 4 Val-CH_3), 2.13 (br.s., 2H, 2 Val-CH), 2.48 (s, 3H, $COCH_3$), 4.32-4.44 (m, 2H, 2 *α*-CH), 6.87-6.96 (m, 2H, 2NH, D_2O exchangeable), 7.82-7.99 (m, 4H, Ar-H), 9.25-9.47 (m, 1H, NH, D_2O exchangeable), 12.33 (br.s., 2H, COOH, D_2O exchangeable); ^{13}C-NMR (125 MHz, DMSO-d_6): δ 19.04, 19.76, 26.84, 30.35, 58.85, 59.31, 116.37, 118.94, 129.66, 145.76, 164.29, 166.12, 166.31, 174.32, 174.48, 196.85. Anal. calcd. for $C_{21}H_{28}N_6O_5$ (%): C, 56.75; H, 6.35; N, 18.91. Found: C, 56.96; H, 6.13; N, 19.01.

*5.1.1.1.3. 2,2'-{[6-(4-Acetylanilino)-1,3,5-triazine-2,4-diyl]diazanediyl}bis(3-phenylpropanoic acid) (**5c**).* White solid, yield: 64.7 % ; m.p. 184-186°C; IR (KBr, cm^{-1}): 3700-2800 (br, OH, acid), 3304 (NH), 1727, 1660 (C=O); ^{1}H-NMR (500 MHz, DMSO-d_6): δ 2.47 (s, 3H, $COCH_3$), 3.00-3.11 (m, 4H, 2 Phe-CH_2), 4.58-4.60 (m, 2H, 2 *α*-CH), 7.08-7.13 (m, 2H, 2NH, D_2O exchangeable), 7.14-7.27 (m, 10H, Ar-H), 7.75-7.91 (m, 4H, Ar-H), 9.34-9.43 (m, 1H, NH,

D_2O exchangeable), 12.73 (br.s., 2H, COOH, D_2O exchangeable); ^{13}C-NMR (125 MHz, DMSO-d_6): δ 26.82, 39.74, 39.90, 55.30, 55.82, 118.89, 119.02, 126.88, 128.73, 129.68, 131.04, 138.57, 138.82, 145.48, 145.67, 164.15, 165.66, 165.89, 174.57, 196.95. Anal. calcd. for $C_{29}H_{28}N_6O_5$: C, 64.43; H, 5.22; N, 15.55. Found: C, 64.12; H, 5.37; N, 15.76.

*5.1.1.1.4. 2,2',2'',2'''-{[6-(4-acetylanilino)-1,3,5-triazine-2,4-diyl}bis(azanetriyl)]tetraacetic acid (**5d**).* White solid, yield: 69.2 %; m.p. 230-232°C; IR (KBr, cm^{-1}): 3600-2800 (br, OH, acid), 3429 (NH), 1706, 1665 (C=O); ^{1}H-NMR (500 MHz, DMSO-d_6): δ 2.47 (s, 3H, $COCH_3$), 4.03, 4.13 (2s, 8H, 4 α-CH_2), 7.72-7.78 (m, 4H, Ar-H), 9.46 (s, 1H, NH, D_2O exchangeable); ^{13}C-NMR (125 MHz, DMSO-d_6): δ 26.86, 55.00, 116.43, 119.08, 129.65, 132.64, 145.78, 164.00, 164.09, 164.98, 173.48, 196.91. Anal. calcd. for $C_{19}H_{20}N_6O_9$ (%): C, 47.90; H, 4.23; N, 17.64. Found: C, 47.64; H, 4.31; N, 17.81.

*5.1.1.2. General procedure for the synthesis of the target 1,3,5-triazinyl chalcones **7-14***

Potassium hydroxide solution (1g, 5 mL) was drop wisely added to an ice cold mixture of **5a-d** (1 mmol) in ethanol (20 mL) and the appropriate aromatic aldehyde **6a** or **6b** (1 mmol). The reaction mixture was stirred at room temperature overnight. After completion of the reaction, the mixture was poured into ice water and neutralized with 1N HCl. The pure precipitated solid product was washed with cold water, filtered and dried.

5.1.1.2.1. (E)-2,2'-{[6-(4-(3-Phenylprop-2-enoyl)anilino)-1,3,5-triazine-2,4-diyl]diazanediyl}diacetic acid (7). Pale yellow solid, yield: 80.9 %; m.p.: 226-228°C; IR (KBr, cm^{-1}): 3700-2650 (br, OH, acid), 3315 (NH), 1703 (C=O), 1650 (C=N); ^{1}H-NMR (500 MHz, DMSO-d_6): δ 3.90 (s, 4H, 2α-CH_2), 7.15-7.43 (m, 5H, Ar-H), 7.68 (d, 1H, J = 15.3 Hz, ethylene C-H), 7.85-7.92 (m, 5H, Ar-H & ethylene C-H), 8.01-8.05 (m, 2H, 2NH, D_2O exchangeable), 9.50 (s, 1H, NH, D_2O exchangeable); ^{13}C-NMR (125 MHz, DMSO-d_6): δ 42.50, 42.74, 119.12, 119.45, 123.37, 129.42, 130.26, 130.96, 134.31, 135.41, 141.99, 145.95, 164.41, 165.20, 165.95, 166.20, 172.41, 187.85. Anal. calcd. for $C_{22}H_{20}N_6O_5$ (%): C, 58.92; H, 4.50; N, 18.74. Found: C, 59.14; H, 4.39; N, 18.79.

*5.1.1.2.2. (E)-2,2'-{[6-(4-(3-(4-Clorophenyl)prop-2-enoyl)anilino)-1,3,5-triazine-2,4-diyl]diazanediyl}diacetic acid (**8**).* Pale yellow solid, yield: 84.9 %; m.p. 244-246°C; IR (KBr, cm^{-1}): 3550-2750 (br, OH, acid), 3323 (NH), 1710 (C=O), 1635 (C=N); ^{1}H-NMR (500 MHz, DMSO-d_6): δ 3.91-3.93 (m, 4H, 2α-CH_2), 7.21-7.50 (m, 4H, Ar-H), 7.66 (d, 1H, J = 15.3 Hz, ethylene C-

H), 7.81-8.00 (m, 5H, Ar-H & ethylene C-H), 8.04-8.06 (m, 2H, 2NH, D_2O exchangeable), 9.50-9.68 (m, 1H, NH, D_2O exchangeable), 12.50 (s, 2H, COOH, D_2O exchangeable); ^{13}C-NMR (125 MHz, DMSO-d_6): δ 42.48, 42.73, 119.11, 119.42, 123.35, 129.47, 130.22, 130.96, 134.36, 135.41, 141.99, 145.94, 164.10, 165.20, 165.85, 166.20, 172.51, 187.77. Anal. calcd. for $C_{22}H_{19}ClN_6O_5$ (%): C, 54.72; H, 3.97; N, 17.40. Found: C, 54.56; H, 4.05; N, 17.28.

*5.1.1.2.3. (E)-2,2'-{[6-(4-(3-Phenylprop-2-enoyl)anilino)-1,3,5-triazine-2,4-diyl]diazanediyl}bis(3-methylbutanoic acid) (**9**).* Pale yellow solid, yield: 70.6 %; m.p. 206-208°C; IR (KBr, cm^{-1}): 3650-2850 (br, OH, acid), 3410 (NH), 1721 (C=O), 1656 (C=N); ^{1}H-NMR (500 MHz, DMSO-d_6): δ 0.94 (br.s., 12H, 4CH_3), 2.13-2.15, 4.33-4.45 (2m, 4H, 4α-CH), 6.90-7.42 (m, 5H, Ar-H), 7.68 (d, 1H, *J* = 15.3 Hz, ethylene C-H), 7.84-8.00 (m, 5H, Ar-H & ethylene C-H), 8.01-8.07 (m, 2H, 2NH, D_2O exchangeable), 9.26-9.53 (m, 1H, NH, D_2O exchangeable); ^{13}C-NMR (125 MHz, DMSO-d_6): δ 19.02, 19.08, 19.78, 30.20, 30.39, 58.93, 59.37, 118.94, 119.13, 122.64, 129.26, 129.45, 130.18, 143.42, 145.69, 145.94, 164.31, 166.14, 166.33, 174.36, 174.55, 187.91. Anal. calcd. for $C_{28}H_{32}N_6O_5$ (%): C, 63.14; H, 6.06; N, 15.78. Found: C, 63.23; H, 6.17; N, 15.54.

*5.1.1.2.4. (E)-2,2'-{[6-(4-(3-(4-Clorophenyl)prop-2-enoyl)anilino)-1,3,5-triazine-2,4-diyl]diazanediyl} bis(3-methylbutanoic acid) (**10**).* Pale yellow solid, yield: 58.9 %; m.p. 236-238°C; IR (KBr, cm^{-1}): 3750-2800 (br, OH, acid), 3406 (NH), 1721 (C=O), 1659 (C=N) cm^{-1}; ^{1}H-NMR (500 MHz, DMSO-d_6): δ 0.93 (br.s., 12H, 4CH_3), 2.14 (br.s., 2H, 2CH), 4.33-4.43 (m, 2H, 2α-CH), 6.92-7.49 (m, 4H, Ar-H), 7.66 (d, 1H, *J* = 13.8 Hz, ethylene C-H), 7.82-7.99 (m, 5H, Ar-H & ethylene C-H), 8.07 (br.s., 2H, 2NH, D_2O exchangeable), 9.27-9.52 (m, 1H, NH, D_2O exchangeable); ^{13}C-NMR (125 MHz, DMSO-d_6): δ 19.04, 19.23, 19.80, 30.45, 58.99, 59.42, 119.08, 129.47, 130.24, 130.96, 134.40, 141.91, 146.59, 159.18, 164.33, 164.40, 166.10, 166.29, 174.53, 174.69, 187.75. Anal. calcd. for $C_{28}H_{31}ClN_6O_5$ (%): C, 59.31; H, 5.51; N, 14.82. Found: C, 59.13; H, 5.72; N, 14.98.

*5.1.1.2.5. (E)-2,2'-{[6-(4-(3-Phenylprop-2-enoyl)anilino)-1,3,5-triazine-2,4-diyl]diazanediyl}bis(3-phenylpropanoic acid) (**11**).* Pale yellow solid, yield: 88.4 %; m.p. 202-205°C; IR (KBr, cm^{-1}): 3700-2500 (br, OH, acid), 3303 (NH), 1724, 1660 (C=O) cm^{-1}; ^{1}H-NMR (500 MHz, DMSO-d_6): δ 3.01-3.14 (m, 4H, 2CH_2), 4.61 (br.s., 2H, 2α-CH), 7.08-7.43 (m, 15H, Ar-H), 7.70 (d, 1H, *J* = 14.5 Hz, ethylene C-H), 7.80-7.92 (m, 5H, Ar-H & ethylene C-H), 8.06

(br.s., 2H, 2NH, D_2O exchangeable), 9.33-9.47 (m, 1H, NH-Ar, D_2O exchangeable); ^{13}C-NMR (125 MHz, DMSO-d_6): δ 37.22, 55.49, 55.87, 119.06, 126.84, 128.69, 129.28, 129.45, 129.59, 129.71, 130.19, 130.93, 135.43, 138.91, 143.43, 145.91, 164.17, 165.90, 166.08, 174.66, 187.87. Anal. calcd. for $C_{36}H_{32}N_6O_5$ (%): C, 68.78; H, 5.13; N, 13.37. Found: C, 69.01; H, 5.03; N, 13.46.

*5.1.1.2.6. (E)-2,2'-{[6-(4-(3-(4-Clorophenyl)prop-2-enoyl)anilino)-1,3,5-triazine-2,4-diyl]diazanediyl} bis(3-phenylpropanoic acid) (**12**).* Pale yellow solid, yield: 75.7 %; m.p. 228-230°C; IR (KBr, cm^{-1}): 3600-2700 (br, OH, acid), 3405 (NH), 1725, 1659 (C=O) cm^{-1}; ^{1}H-NMR (500 MHz, DMSO-d_6): δ 3.02-3.16 (m, 4H, 2CH_2), 4.60 (br.s, 2H, 2α-CH), 7.12-7.49 (m, 14H, Ar-H), 7.67 (d, 1H, *J* = 13.8 Hz, ethylene C-H), 7.80-7.98 (m, 5H, Ar-H & ethylene C-H), 8.07 (br.s, 2H, 2NH, D_2O exchangeable), 9.36-9.47 (m, 1H, NH, D_2O exchangeable); ^{13}C-NMR (125 MHz, DMSO-d_6): δ 37.20, 55.65, 56.16, 117.25, 118.96, 123.38, 126.72, 128.57, 129.47, 129.75, 130.27, 131.01, 134.41, 135.37, 139.02, 141.98, 164.20, 164.36, 165.75, 174.97, 187.70. Anal. calcd. for $C_{36}H_{31}ClN_6O_5$: C, 65.21; H, 4.71; N, 12.67. Found: C, 64.98; H, 4.63; N, 12.81.

*5.1.1.2.7. (E)-2,2'-{[6-(4-(3-Phenylprop-2-enoyl)anilino)-1,3,5-triazine-2,4 diyl}bis(azanetriyl)]tetraacetic acid (**13**).* Pale yellow solid, yield: 53.1 %; m.p. > 300°C; IR (KBr, cm^{-1}): 3700-2900 (br, OH, acid), 3408 (NH), 1723 (C=O), 1645 (C=N); ^{1}H-NMR (500 MHz, DMSO-d_6): δ 4.09-4.16 (m, 8H, 4α-CH_2), 6.91-7.43 (m, 5H, Ar-H), 7.68 (d, 1H, *J* = 15.3 Hz, ethylene C-H), 7.76-8.03 (m, 5H, Ar-H & ethylene C-H), 9.48-9.58 (m, 1H, NH, D_2O exchangeable); ^{13}C-NMR (125 MHz, DMSO-d_6): δ 51.34, 51.55, 119.06, 119.27, 122.61, 128.86, 129.28, 129.47, 141.99, 164.14, 165.15, 172.99, 173.22, 187.51. Anal. calcd. for $C_{26}H_{24}N_6O_9$ (%): C, 55.32; H, 4.29; N, 14.89. Found: C, 55.61; H, 4.08; N, 15.01.

*5.1.1.2.8. (E)-2,2'-{[6-(4-(3-(4-Clorophenyl)prop-2-enoyl)anilino)-1,3,5-triazine-2,4-diyl] bis(azanetriyl)]tetraacetic acid (**14**)*. Pale yellow solid, yield: 45.4 %; m.p. > 300°C; IR (KBr, cm^{-1}): 3650-2700 (br, OH, acid), 3400 (NH), 1729 (C=O), 1658 (C=N); ^{1}H-NMR (500 MHz, DMSO-d_6): δ 4.14-4.23 (m, 8H, 4CH_2), 6.91-7.50 (m, 4H, Ar-H), 7.68 (d, 1H, *J* = 15.3 Hz, ethylene C-H), 7.79-8.05 (m, 5H, Ar-H, ethylene C-H), 9.49-9.61 (m, 1H, NH, D_2O exchangeable), 13.21 (m, 2H, 2COOH, D_2O exchangeable); ^{13}C-NMR (125 MHz, DMSO-d_6): δ 51.56, 51.76, 119.25, 123.37, 129.47, 130.20, 130.99, 133.27, 134.40, 134.62, 135.37, 141.99, 163.93, 164.14, 165.24, 172.61, 172.68, 187.51. Anal. calcd. for $C_{26}H_{23}ClN_6O_9$ (%): C, 52.14; H, 3.87; N, 14.03. Found: C, 51.97; H, 4.01; N, 13.91.

5.1.2. Chromatographic conditions

An Agilent 1260 Infinity HPLC system equipped with a quaternary pump, an autosampler, DAD (Diode Array Detector), and an Agilent Chemstation data processing system was used for the analysis. The HPLC analysis was carried out with an Agilent Zorbax Eclipse XDB C_{18} reversed-phase column (250×4.6 mm, 5 μm particle size) maintained at room temperature. The injection volume was 30 μL. The mobile phase consisted of 70%:30% acetonitrile: water. Total run time was 8 minutes pumped at flow rate 1 mL/min. Compound **5c** was detected at 300 nm with a retention time of 2.7 (93.8%) and 2.9 (6.2%) min. Compound **12** was detected at 320 nm with a retention time of 6.2 (92.1%) and 6.5 (7.1%) min.

5.2. Antitumor and Cytotoxicity evaluation by MTT assay

5.2.1. Percent cell viability determination

A549 lung cancer cell line was purchased from the Medical Research Institute (MRI), Alexandria University, Alexandria, Egypt. Cells were cultured in high glucose Dulbecco's Modified Eagle's Medium (DMEM) (with L-Glutamine) (Lonza, Belgium) containing 10% fetal bovine serum (FBS) (Sigma, Germany) in 10 cm cell culture dishes. Incubation of cultures was carried out in humidified CO_2 incubator (Shel Lab, USA) (5% CO_2, 37°C). Experiments were performed with cultures of 70-80% confluence with a maximum passage number of 20. Cells were seeded in 96-well plates at a density of 10^4 cell/well and were supplemented with 200 μL DMEM containing 10% FBS. After 24 h, the culture medium was aspirated and replaced with fresh complete medium containing 500 μM of the tested compounds dissolved in DMSO using DMSO-treated cultures as control. Also, combined treatment of each of the tested compounds with cisplatin (VANEX S.A., Greece) was prepared (10 μg/ml). After 48 h, wells were washed with phosphate buffered saline (PBS) containing 2.5 mg/ml of 3-(4,5-dimethylthiazol-2-yl)-2,5-diphenyltetrazolium bromide (MTT) (SERVA, Germany) in serum-free DMEM. After 2 h of incubation, excess MTT reagent were carefully aspirated from the wells and 100 μL DMSO was added into each well for 15 min to dissolve the MTT formazan. Absorbance readings were recorded at 540 nm using a microplate reader. The following formula was used to calculate the percent of cell viability (%) = Absorbance of treated cells/ Absorbance of control cells x 100. Data were expressed as mean ± standard

deviation (SE) of two independent repeats. Student's *t*-test was applied for evaluating the data significance using Microsoft Excel 2016. Results were considered statistically significant when *p* value < 0.05.

5.2.2. IC_{50} determination

Lung adenocarcinoma cell line A549 was obtained from ATCC and cultured in DMEM high glucose medium (4.5g/L) supplemented with 10% FBS and 1% Penicillin/Streptomycin at 37°C and 5% CO_2. Normal human fibroblasts isolated from the gingiva were obtained from CERRMA, Faculty of Medicine, Alexandria University. They were cultured in DMEM low glucose medium supplemented with 10% FBS and 1% Penicillin/Streptomycin. Cells were treated with either cisplatin (3.33μM, 6.66 μM, 13.32 μM, 33.33 μM and 66.6 μM) or compound **10** (1.76 μM, 3.53 μM, 7.05 μM, 17.6 μM, and 35.27 μM) and **12** (1.51 μM, 3.02 μM, 6.03 μM, 15.08 μM, and 30.16 μM) and seeded in 96-well plate at a seeding density of $1x10^4$ cells/well. After 24 h, the medium was replaced with another containing different concentrations of either cisplatin or the test compounds for 48 h, respectively. The corresponding culture medium was used as an empty control. To measure the cytotoxicity of the test compounds and cisplatin individually, 10 µl of 5 mg/mL 3-(4,5-dimethylthiazol-2-yl)-2,5-diphenyltetrazolium bromide (MTT, Serva) solution was added to each well and incubated for 4 h at 37 ˚C. The supernatant was then discarded from each well and DMSO (100 µL) was added to dissolve the formazan crystals. Absorbance was measured at 570 nm with a microplate reader (Tecan, USA). The concentrations causing 50% inhibition of cell viability (IC_{50}) were calculated form sigmoidal dose-response curve-fitting graphs.

*5.2.3. Combined antitumor and cytotoxicity response of cisplatin with **10** and **12***

The antitumor effects of all combinations were determined after 48 h incubation period using MTT assay. Three different equipotent concentrations for each binary combination were tested in six replicates**.** The CI was determined using the Chou-Talalay method. For the CI analysis, we considered that both tested compounds have independent mechanism of action for the induction of cell death. Calculation of the CI values were done to define the nature of compound interaction using the following equation: $CIx = (D1/Dx1)+(D2/Dx2)$, where CIx represents the CI value for 50% cell viability, Dx1 and Dx2 represent the doses of compounds **10** and **12** required to exert 50% effect alone, and D1 and D2 represent the doses of **10** and **12** that elicit the same 50% effect

in combination with cisplatin, respectively. In addition, the Dose Reduction Index (DRI) was calculated and the dose-effect curve was constructed for each single drug utilizing the CompuSyn software program (ComboSyn Inc., Paramus, NJ. U.S.A). Inhibitory concentration for 50% of the cells ($IC_{50,}$ D_m), the linear correlation coefficient (r) of each dose-effect curve and the sigmoidicity coefficient (m) were calculated utilizing the same software program based on the Median-Effect Equation. The effect of equipotent binary combinations of cisplatin with compound **10** or **12** on the cell viability of normal human fibroblast cells were investigated in the same manner described above.

5.3. DNA Binding studies

5.3.1. Materials

The synthetic dsDNA sequence, 5'– GTC GCA CGG CAC GGA TAG GTA – 3', 3'–CAG CGT GCC GTG CCT ATC CAT– 5' was obtained from Bio Basic Canada Inc. (Ontario, Canada) and was purified by standard desalting. The calf thymus DNA (ctDNA) was obtained from Sigma-Aldrich Canada Ltd. (Oakville, Ontario). The EvaGreen (EG) dye was purchased from Biotium Inc. (Fremont, California), sodium chloride was obtained from EMD Chemicals Inc. (Gibbstown, New Jersey), Tris was obtained from ICN Biomedicals, (Aurora, Ohio) and ethylenediaminetetraacetic acid (EDTA) was purchased from BDH Inc. (Toronto, Ontario). All chemicals were used as received. Synthetic dsDNA solutions were prepared in Tris buffer solution (10 mM Tris, 10 mM NaCl, 1 mM EDTA, pH 7.5) at the concentrations indicated for each experiment then gradually heated to a temperature of 85°C in a water bath and annealed at room temperature (25 °C) in the dark for 24 h before use for all samples. Compounds **10** and **12** (500 μM) were dissolved in 50% DMSO: 50% H_2O.

5.3.2. MALDI-TOF mass spectrometry

Reaction mixtures of 50 μM of the dsDNA sequence with 500 μM of each of **10** and **12** ([dsDNA]: [test compound] = 1:10), in absence and presence of cisplatin (10 μg/ml), were incubated at room temperature for 24 h. After incubation, each reaction mixture was loaded onto a sample plate with the matrix 9:1 (2,4,6-trihydroxyacetophenone/diammonium citrate) and measured by a MALDI-TOF-Mass spec-Elite Voyager equipped with a nitrogen laser for ionization and desorption. The nitrogen laser operated at 337 nm with 3 ns pulse delivered to a sample at 20 Hz.

5.3.3. Fluorescence measurements

For measuring the rate of DNA damage induced by **10** and **12** in absence and presence of cisplatin, 0.2 μM of the synthetic dsDNA was mixed separately with 0.3 μM EG dye using buffer (10 mM Tris, 10 mM NaCl, 1mM EDTA, pH 7.5) in different 96-well microplates. The microplates were incubated at 37 °C for 20 min in the dark and left to cool for 1 h at room temperature, then 10 μM of **10** and **20** were added separately to dsDNA-EG mixture in separate wells. For measuring the DNA damaging effect in presence of cisplatin, cisplatin was added to the specified wells to reach a final concentration of 0.2 μM dsDNA, 0.3μM EG, 10 μM of **10** or **12** and 5 μM cisplatin in buffer (10mM Tris, 10mM NaCl, 1 mM EDTA, pH 7.5). Room temperature fluorescence intensities were recorded every minute for a period of 24 h using the Safire fluorescence plate reader with an excitation wavelength of 490 nm and an emission wavelength of 530 nm.

For calf thymus DNA (ctDNA) experiment, 0.01 μM ctDNA was mixed with different concentrations of each chemical compound **10** and **12** (0 – 100 μM). After incubation with 2.0 μM EG dye using buffer (10 mM Tris, 10 mM NaCl, 1mM EDTA, pH 7.5) in different 96-well microplates at 37 °C for 20 min in the dark and left to cool for 1 h at room temperature. The fluorescence spectra between 500 and 650 nm with excitation at 490 nm were measured. For measuring the DNA damaging effect in presence of cisplatin, 10 μM cisplatin was added to other aliquots, and the same procedure was repeated.

5.4. Binding mode analysis (Molecular docking)

The three dimentional structure of DNA dodecamer co-crystallized with its original ligand distamycin was obtained from the protein databank, PDB ID: 2DND (https://www.rcsb.org/). Molecular Orbital Environment software (MOE version 2016.08.02) was employed to prepare the raw DNA by deleting the crystallized free water molecules and adjusting missing loops. Structure integrity was checked and the active pocket was fixed using Active Site Finder tool to be further used for the docking study. Validation was done by redocking of distamycin in the active pocket with RMSD < 2Å. Test compounds were energy minimized and docked employing the MOE dock tool into the active binding site using induced fit sampling. Triangular matcher algorithm was set as the ligand placement method while London dG was the default scoring function to generate the top five non-redundant poses for each ligand. Based on the energy binding score, the best-docked

structure for each ligand was determined and inspection of the 2D and 3D ligand interactions were performed in reference to the original ligand.

5.5. Apoptosis assay by flow cytometry

The type of cell death (apoptosis/necrosis) induced by the test compounds was determined using Annexin V-FITC/ PI double staining. Briefly, A549 cells ($3x10^5$/well) were plated in 6-well plates and cultured overnight. Subsequently, cells were treated with cisplatin (21.5 µM) alone or in combination with either compounds **10** (24.5 µM) or **12** (17 µM). Cells were harvested after 24 h incubation with the compounds and untreated cells were used as control. For Annexin V-FITC/ PI apoptosis analysis, the cells were suspended in 500 µL of binding buffer and adjusted to $1x10^6$/mL. Staining solutions containing 5 µL Annexin V-fluorescein isothiocyanate (FITC) and 5 µL propidium iodide (PI) (BD Biosciences) were added to the cells and then incubated at a temperature of 2-8˚C for 15 min in the dark. Finally, cells were analyzed using a FACS Calibur flow cytometer (Becton Dickinson, Franklin Lakes, NJ, USA). The percent of viable, early apoptotic, late apoptotic and necrotic cells were evaluated using CellQuest software version 5.1 (BD Biosciences, San Jose, CA, USA). Results were presented as dot plots. Data represented are the mean values ± SEM for three independent experiments. Statistical significance was assessed by two-way ANOVA test.

Declaration of interests

The authors thereby declare that they have neither known competing interest financial interests nor personal relationships that could have influenced the work reported in this paper.

Acknowledgement

The authors are thankful to L'Oréal-UNESCO for Women in Science Egypt Programme for supporting the spectrometric part of this work.

References

[1] F. Bray, J. Ferlay, I. Soerjomataram, R.L. Siegel, L.A. Torre, A. Jemal, Global cancer statistics 2018: GLOBOCAN estimates of incidence and mortality worldwide for 36 cancers in 185 countries, CA. Cancer J. Clin. 68 (2018) 394–424. doi:10.3322/caac.21492.

[2] D. Planchard, S. Popat, K. Kerr, S. Novello, E.F. Smit, C. Faivre-Finn, T.S. Mok, M. Reck, P.E. Van Schil, M.D. Hellmann, S. Peters, E.G. Committee, Metastatic non-small cell lung cancer: ESMO Clinical Practice Guidelines for diagnosis, treatment and follow-up†, Ann. Oncol. 29 (2018) iv192-iv237. doi:10.1093/annonc/mdy275.

[3] C.-Y. Huang, D.-T. Ju, C.-F. Chang, P. Muralidhar Reddy, B.K. Velmurugan, A review on the effects of current chemotherapy drugs and natural agents in treating non-small cell lung cancer, BioMedicine. 7 (2017) 23. doi:10.1051/bmdcn/2017070423.

[4] L.H. Hurley, DNA and Associated Targets for Drug Design, J. Med. Chem. 32 (1989) 2027–2033. doi:10.1021/jm00129a001.

[5] G.M. Boike, E. Petru, B.U. Sevin, H.E. Averette, T.C. Chou, M. Penalver, D. Donato, M. Schiano, S.G. Hilsenbeck, J. Perras, Chemical enhancement of cisplatin cytotoxicity in a human ovarian and cervical cancer cell line, Gynecol. Oncol. 38 (1990) 315–322. doi:10.1016/0090-8258(90)90065-S.

[6] J.-N. Ho, S.-S. Byun, S. Lee, J.J. Oh, S.K. Hong, S.E. Lee, J.S. Yeon, Synergistic Antitumor Effect of Triptolide and Cisplatin in Cisplatin Resistant Human Bladder Cancer Cells, J. Urol. 193 (2015) 1016–1022. doi:https://doi.org/10.1016/j.juro.2014.09.007.

[7] S. Ali, M. Tahir, A.A. Khan, C.X. Chen, M. Ling, Y. Huang, Cisplatin Synergistically Enhances Antitumor Potency of Conditionally Replicating Adenovirus via p53 Dependent or Independent Pathways in Human Lung Carcinoma, Int. J. Mol. Sci. . 20 (2019). doi:10.3390/ijms20051125.

[8] R.Y. Chuang, J.S. Ramlet, H.C. Harder, Biochemical studies on the potentiation of antitumor activity of cisplatin by adriamycin, Biochem. Biophys. Res. Commun. 115 (1983) 577–582. doi:10.1016/S0006-291X(83)80183-1.

[9] J. Sastry, S.J. Kellie, SEVERE NEUROTOXICITY, OTOTOXICITY AND NEPHROTOXICITY FOLLOWING HIGH-DOSE CISPLATIN AND AMIFOSTINE, Pediatr. Hematol. Oncol. 22 (2005) 441–445. doi:10.1080/08880010590964381.

[10] R.P. Miller, R.K. Tadagavadi, G. Ramesh, W.B. Reeves, Mechanisms of Cisplatin Nephrotoxicity, Toxins (Basel). 2 (2010) 2490–2518. doi:10.3390/toxins2112490.

[11] A. De Luca, L.J. Parker, W.H. Ang, C. Rodolfo, V. Gabbarini, N.C. Hancock, F. Palone, A.P. Mazzetti, L. Menin, C.J. Morton, M.W. Parker, M. Lo Bello, P.J. Dyson, A structure-based mechanism of cisplatin resistance mediated by glutathione transferase P1-1, Proc. Natl. Acad. Sci. U. S. A. 116 (n.d.) 13943–13951. doi:10.1073/pnas.1903297116.

[12] X. Huang, M. Wang, C. Wang, W. Hu, Q. You, Y. Yang, C. Yu, Z. Liao, S. Gou, H. Wang, Dual-targeting antitumor conjugates derived from platinum(IV) prodrugs and microtubule inhibitor CA-4 significantly exhibited potent ability to overcome cisplatin resistance, Bioorg. Chem. 92 (2019) 103236. doi:10.1016/j.bioorg.2019.103236.

[13] T.-C. Chou, Theoretical Basis, Experimental Design, and Computerized Simulation of Synergism and Antagonism in Drug Combination Studies, Pharmacol. Rev. 58 (2006) 621 LP-681. doi:10.1124/pr.58.3.10.

[14] H. Wu, H. Jin, C. Wang, Z. Zhang, H. Ruan, L. Sun, C. Yang, Y. Li, W. Qin, C. Wang, Synergistic Cisplatin/Doxorubicin Combination Chemotherapy for Multidrug-Resistant Cancer via Polymeric Nanogels Targeting Delivery, ACS Appl. Mater. Interfaces. 9 (2017) 9426–9436. doi:10.1021/acsami.6b16844.

[15] C.J.A. Van Moorsel, H.M. Pinedo, G. Veerman, A.M. Bergman, C.M. Kuiper, J.B.

Vermorken, W.J.F. Van Der Vijgh, G.J. Peters, Mechanisms of synergism between cisplatin and gemcitabine in ovarian and non small-cell lung cancer cell lines, Br. J. Cancer. 80 (1999) 981–990. doi:10.1038/sj.bjc.6690452.

[16] T. Sugiyama, M. Yakushiji, Y. Aoki, K. Tanaka, R. Nishimura, K. Hasegawa, M. Ikeda, K. Noda, B.-181339 O.C.S. Group, Paclitaxel-cisplatin combination in advanced ovarian cancer: a phase II study, Int. J. Clin. Oncol. 5 (2000) 85–88. doi:10.1007/s101470050096.

[17] A. Jarzab, J. Łuszczki, M. Guz, K. Skalicka-Wozniak, M. Halasa, J. Smok-Kalwat, K. Polberg, A. Stepulak, Combination of Osthole and Cisplatin Against Rhabdomyosarcoma TE671 Cells Yielded Additive Pharmacologic Interaction by Means of Isobolographic Analysis, Anticancer Res. 38 (2018) 205–210. http://ar.iiarjournals.org/content/38/1/205.abstract.

[18] X. Li, S. Guo, X.-K. Xiong, B.-Y. Peng, J.-M. Huang, M.-F. Chen, F.-Y. Wang, J.-N. Wang, Combination of quercetin and cisplatin enhances apoptosis in OSCC cells by downregulating xIAP through the NF-κB pathway, J. Cancer. 10 (2019) 4509–4521. doi:10.7150/jca.31045.

[19] P. Baharuddin, N. Satar, K.S. Fakiruddin, N. Zakaria, M.N. Lim, N.M. Yusoff, Z. Zakaria, B.H. Yahaya, Curcumin improves the efficacy of cisplatin by targeting cancer stem-like cells through p21 and cyclin D1-mediated tumour cell inhibition in non-small cell lung cancer cell lines, Oncol. Rep. 35 (2016) 13–25. doi:10.3892/or.2015.4371.

[20] Y. Oda, M. Hidaka, A. Suzuki, Caffeine Has a Synergistic Anticancer Effect with Cisplatin *via* Inhibiting Fanconi Anemia Group D2 Protein Monoubiquitination in Hepatocellular Carcinoma Cells, Biol. Pharm. Bull. 40 (2017) 2005–2009. doi:10.1248/bpb.b17-00457.

[21] J.R. Perussi, D.N. Paltoo, V.A.L. Toppin, R.G. Canada, Synergism between dipyridamole and cisplatin in human breast cancer cells in vitro, Quim. Nova. 26 (2003) 340–343. doi:10.1590/S0100-40422003000300010.

[22] I. Gonzalez-Sanchez, A. Lira-Rocha, A. Navarrete, M.A. Loza-Mejia, C. Coronel-Cruz, C.A. Mendoza-Rodriguez, M.A. Cerbon, Synergistic Anticancer Activity of Thiazolo[5,4-b]quinoline Derivative D3CLP in Combination with Cisplatin in Human Cervical Cancer Cells, Anticancer Res. 32 (2012) 5159–5165. http://ar.iiarjournals.org/content/32/12/5159.abstract.

[23] A. Macieja, P. Kopa, G. Galita, E. Pastwa, I. Majsterek, T. Poplawski, Comparison of the effect of three different topoisomerase II inhibitors combined with cisplatin in human glioblastoma cells sensitized with double strand break repair inhibitors, Mol. Biol. Rep. 46 (2019) 3625–3636. doi:10.1007/s11033-019-04605-0.

[24] M.M. Georgiadis, Q. Chen, J. Meng, C. Guo, R. Wireman, A. Reed, M.R. Vasko, M.R. Kelley, Small molecule activation of apurinic/apyrimidinic endonuclease 1 reduces DNA damage induced by cisplatin in cultured sensory neurons, DNA Repair (Amst). 41 (2016) 32–41. doi:https://doi.org/10.1016/j.dnarep.2016.03.009.

[25] A. Marczak, B. Bukowska, A. Rogalska, WP 631 and Epo B synergize in SKOV-3 human ovarian cancer cells, Environ. Toxicol. Pharmacol. 37 (2014) 256–266. doi:https://doi.org/10.1016/j.etap.2013.12.002.

[26] S. Cascioferro, B. Parrino, V. Spanò, A. Carbone, A. Montalbano, P. Diana, G. Cirrincione, 1,3,5-Triazines: A promising scaffold for anticancer drugs development, Eur. J. Med. Chem. 142 (2017) 523–549. doi:10.1016/J.EJMECH.2017.09.035.

[27] J.K. Chan, V. Loizzi, A. Manetta, M.L. Berman, Oral altretamine used as salvage therapy in recurrent ovarian cancer, Gynecol. Oncol. 92 (2004) 368–371. doi:10.1016/j.ygyno.2003.09.017.

[28] H. Guan, B. Mi, Y. Li, W. Wu, P. Tan, Z. Fang, J. Li, Y. Zhang, F. Li, Decitabine represses osteoclastogenesis through inhibition of RANK and NF-κB, Cell. Signal. 27 (2015) 969–977. doi:https://doi.org/10.1016/j.cellsig.2015.02.006.

[29] O. Salim, T. Toptas, E. Avsar, O.K. Yucel, E. Ozturk, B. Ferhanoglu, A. Geduk, O. Mehtap, A. Tombak, E.N. Tiftik, B. Deveci, E. Kurtoglu, O. Kara, I.K. Atagunduz, T.F. Tuglular, L. Undar, Azacitidine versus decitabine in patients with refractory anemia with excess blast—Results of multicenter study, Leuk. Res. 45 (2016) 82–89. doi:10.1016/J.LEUKRES.2016.04.003.

[30] S.-M. Maira, S. Pecchi, A. Huang, M. Burger, M. Knapp, D. Sterker, C. Schnell, D. Guthy, T. Nagel, M. Wiesmann, S. Brachmann, C. Fritsch, M. Dorsch, P. Chène, K. Shoemaker, A. De Pover, D. Menezes, G. Martiny-Baron, D. Fabbro, C.J. Wilson, R. Schlegel, F. Hofmann, C. García-Echeverría, W.R. Sellers, C.F. Voliva, Identification and Characterization of NVP-BKM120, an Orally Available Pan-Class I PI3-Kinase Inhibitor, Mol. Cancer Ther. 11 (2012) 317 LP-328. doi:10.1158/1535-7163.MCT-11-0474.

[31] D. Kong, T. Yamori, ZSTK474 is an ATP-competitive inhibitor of class I phosphatidylinositol 3 kinase isoforms, Cancer Sci. 98 (2007) 1638–1642. doi:10.1111/j.1349-7006.2007.00580.x.

[32] M. Zheng, C. Xu, J. Ma, Y. Sun, F. Du, H. Liu, L. Lin, C. Li, J. Ding, K. Chen, H. Jiang, Synthesis and antitumor evaluation of a novel series of triaminotriazine derivatives, Bioorg. Med. Chem. 15 (2007) 1815–1827. doi:https://doi.org/10.1016/j.bmc.2006.11.028.

[33] A.B. Patel, K.H. Chikhalia, P. Kumari, An efficient synthesis of new thiazolidin-4-one fused s-triazines as potential antimicrobial and anticancer agents, J. Saudi Chem. Soc. 18 (2014) 646–656. doi:https://doi.org/10.1016/j.jscs.2014.02.002.

[34] Q. Huang, Q. Fu, Y. Liu, J. Bai, Q. Wang, H. Liao, P. Gong, Design, synthesis and anticancer activity of novel 6-(aminophenyl)-2,4-bismorpholino-1,3,5-triazine derivatives bearing arylmethylene hydrazine moiety, Chem. Res. Chinese Univ. 30 (2014) 257–265. doi:10.1007/s40242-014-3253-5.

[35] J.K. Srivastava, G.G. Pillai, H.R. Bhat, A. Verma, U.P. Singh, Design and discovery of novel monastrol-1,3,5-triazines as potent anti-breast cancer agent via attenuating Epidermal Growth Factor Receptor tyrosine kinase, Sci. Rep. 7 (2017) 5851. doi:10.1038/s41598-017-05934-5.

[36] H.M.E. Marwa I. Serag, Rania, M. Gomaa, Mohammed A. M. Massoud, Design, Synthesis and Molecular Modeling of New 1,3,5-Triazine Derivatives as Anticancer Agents, Der Pharma Chem. 11 (2019) 7–14.

[37] C. Zhuang, W. Zhang, C. Sheng, W. Zhang, C. Xing, Z. Miao, Chalcone: A Privileged Structure in Medicinal Chemistry, Chem. Rev. 117 (2017) 7762–7810. doi:10.1021/acs.chemrev.7b00020.

[38] N. Shankaraiah, K.P. Siraj, S. Nekkanti, V. Srinivasulu, P. Sharma, K.R. Senwar, M. Sathish, M.V.P.S. Vishnuvardhan, S. Ramakrishna, C. Jadala, N. Nagesh, A. Kamal, DNA-binding affinity and anticancer activity of β-carboline–chalcone conjugates as potential DNA intercalators: Molecular modelling and synthesis, Bioorg. Chem. 59 (2015) 130–139. doi:https://doi.org/10.1016/j.bioorg.2015.02.007.

[39] S. Gupta, G.E.N. Kass, E. Szegezdi, B. Joseph, The mitochondrial death pathway: a promising therapeutic target in diseases, J. Cell. Mol. Med. 13 (2009) 1004–1033. doi:10.1111/j.1582-4934.2009.00697.x.

[40] T. Sakai, R.N. Eskander, Y. Guo, K.J. Kim, J. Mefford, J. Hopkins, N.N. Bhatia, X. Zi, B.H. Hoang, Flavokawain B, a kava chalcone, induces apoptosis in synovial sarcoma cell lines, J. Orthop. Res. 30 (2012) 1045–1050. doi:10.1002/jor.22050.

[41] M. Hossain, U. Das, J.R. Dimmock, Recent advances in α,β-unsaturated carbonyl compounds as mitochondrial toxins, Eur. J. Med. Chem. 183 (2019) 111687. doi:10.1016/J.EJMECH.2019.111687.

[42] B. Srinivasan, T.E. Johnson, R. Lad, C. Xing, Structure - Activity relationship studies of chalcone leading to 3-hydroxy-4,3′,4′,5′-tetramethoxychalcone and its analogues as potent nuclear factor κB inhibitors and their anticancer activities, J. Med. Chem. 52 (2009) 7228–7235. doi:10.1021/jm901278z.

[43] D. Kumar, N.M. Kumar, K. Akamatsu, E. Kusaka, H. Harada, T. Ito, Synthesis and biological evaluation of indolyl chalcones as antitumor agents, Bioorg. Med. Chem. Lett. 20 (2010) 3916–3919. doi:https://doi.org/10.1016/j.bmcl.2010.05.016.

[44] S.-H. Kim, E. Lee, K.H. Baek, H.B. Kwon, H. Woo, E.-S. Lee, Y. Kwon, Y. Na, Chalcones, inhibitors for topoisomerase I and cathepsin B and L, as potential anti-cancer agents, Bioorg. Med. Chem. Lett. 23 (2013) 3320—3324. doi:10.1016/j.bmcl.2013.03.106.

[45] G. Loch-Neckel, M.A. Bicca, P.C. Leal, A. Mascarello, J.M. Siqueira, J.B. Calixto, In vitro and in vivo anti-glioma activity of a chalcone-quinoxaline hybrid, Eur. J. Med. Chem. 90 (2015) 93–100. doi:https://doi.org/10.1016/j.ejmech.2014.11.014.

[46] H.-N. Gil, D. Koh, Y. Lim, Y.H. Lee, S.Y. Shin, The synthetic chalcone derivative 2-hydroxy-3′,5,5′-trimethoxychalcone induces unfolded protein response-mediated apoptosis in A549 lung cancer cells, Bioorg. Med. Chem. Lett. 28 (2018) 2969–2975. doi:https://doi.org/10.1016/j.bmcl.2018.07.003.

[47] G. Wang, W. Liu, Z. Gong, Y. Huang, Y. Li, Z. Peng, Synthesis, biological evaluation, and molecular modelling of new naphthalene-chalcone derivatives as potential anticancer agents on MCF-7 breast cancer cells by targeting tubulin colchicine binding site, J. Enzyme Inhib. Med. Chem. 35 (2020) 139–144. doi:10.1080/14756366.2019.1690479.

[48] L. Moreno, J. Quiroga, R. Abonia, J. Ramírez-Prada, B. Insuasty, Synthesis of New 1,3,5-Triazine-Based 2-Pyrazolines as Potential Anticancer Agents, Molecules. 23 (2018) 1956.

doi:10.3390/molecules23081956.

[49] M.H. El-Wakil, A.F. El-Yazbi, H.M.A. Ashour, M.A. Khalil, K.A. Ismail, I.M. Labouta, Discovery of a novel DNA binding agent via design and synthesis of new thiazole hybrids and fused 1,2,4-triazines as potential antitumor agents: Computational, spectrometric and in silico studies, Bioorg. Chem. 90 (2019). doi:10.1016/j.bioorg.2019.103089.

[50] N.S. Haiba, H.H. Khalil, M.A. Moniem, M.H. El-Wakil, A.A. Bekhit, Sh.N. Khattab, Design, synthesis and molecular modeling studies of new series of s-triazine derivatives as antimicrobial agents against multi-drug resistant clinical isolates, Bioorg. Chem. 89 (2019) 103013–103024. doi:https://doi.org/10.1016/j.bioorg.2019.103013.

[51] D.R. Ramadan, A.A. Elbardan, A.A. Bekhit, A. El-Faham, Sh.N. Khattab, Synthesis and characterization of novel dimeric s-triazine derivatives as potential anti-bacterial agents against MDR clinical isolates, New J. Chem. 42 (2018) 10676–10688. doi:10.1039/C8NJ01483C.

[52] K.M. Al-Zaydi, H.H. Khalil, A. El-Faham, Sh.N. Khattab, Synthesis, characterization and evaluation of 1,3,5-triazine aminobenzoic acid derivatives for their antimicrobial activity, Chem. Cent. J. 11 (2017) 39–51. doi:10.1186/s13065-017-0267-3.

[53] W. Yan, Y. Zhao, J. He, Anti-breast cancer activity of selected 1,3,5-triazines via modulation of EGFR-TK, Mol. Med. Rep. 18 (2018) 4175–4184. doi:10.3892/mmr.2018.9426.

[54] H. Kothayer, A.A. Elshanawani, M.E. Abu Kull, O.I. El-Sabbagh, M.P.V. Shekhar, A. Brancale, A.T. Jones, A.D. Westwell, Design, synthesis and in vitro anticancer evaluation of 4,6-diamino-1,3,5-triazine-2-carbohydrazides and -carboxamides, Bioorg. Med. Chem. Lett. 23 (2013) 6886–6889. doi:10.1016/J.BMCL.2013.09.087.

[55] X. Zarate, E. Schott, C.A. Escobar, R. Lopez-Castro, C. Echeverria, L. Alvarado-Soto, R. Ramirez-Tagle, X. Zarate, E. Schott, C.A. Escobar, R. Lopez-Castro, C. Echeverria, L. Alvarado-Soto, R. Ramirez-Tagle, Interaction of chalcones with CT-DNA by spectrophotometric analysis and theoretical simulations, Quim. Nova. 39 (2016) 914–918. doi:10.5935/0100-4042.20160114.

[56] M. Wan, L. Xu, L. Hua, A. Li, S. Li, W. Lu, Y. Pang, C. Cao, X. Liu, P. Jiao, Synthesis and evaluation of novel isoxazolyl chalcones as potential anticancer agents, Bioorg. Chem. 54 (2014) 38–43. doi:https://doi.org/10.1016/j.bioorg.2014.03.004.

[57] A. Shiekhzadeh, N. Sohrabi, M.E. Moghadam, M. Oftadeh, Kinetic and Thermodynamic Investigation of Human Serum Albumin Interaction with Anticancer Glycine Derivative of Platinum Complex by Using Spectroscopic Methods and Molecular Docking, Appl. Biochem. Biotechnol. 190 (2020) 506–528. doi:10.1007/s12010-019-03078-y.

[58] G. Sosnovsky, I. Prakash, N.U.M. Rao, In the search for new anticancer drugs. XXIV: Synthesis and anticancer activity of amino acids and dipeptides containing the 2-chloroethyl- and [N′-(2-chloroethyl)-N′-nitroso]-aminocarbonyl groups, J. Pharm. Sci. 82 (1993) 1–10. doi:10.1002/jps.2600820102.

[59] S. Chattopadhyay, S.K. Dash, S. Tripathy, P. Pramanik, S. Roy, Phosphonomethyl

iminodiacetic acid-conjugated cobalt oxide nanoparticles liberate Co++ ion-induced stress associated activation of TNF-α/p38 MAPK/caspase 8-caspase 3 signaling in human leukemia cells, JBIC J. Biol. Inorg. Chem. 20 (2015) 123–141. doi:10.1007/s00775-014-1221-7.

[60] Sh.N. Khattab, H.H. Khalil, A.A. Bekhit, M.M. Abd El-Rahman, B.G. de la Torre, A. El-Faham, F. Albericio, 1,3,5-Triazino Peptide Derivatives: Synthesis, Characterization, and Preliminary Antileishmanial Activity, ChemMedChem. 13 (2018) 725–735. doi:10.1002/cmdc.201700770.

[61] Sh.N. Khattab, H.H. Khalil, A.A. Bekhit, M.M.A. El-Rahman, A. El-Faham, F. Albericio, Synthesis and Preliminary Biological Evaluation of 1,3,5-Triazine Amino Acid Derivatives to Study Their MAO Inhibitors, Molecules. 20 (2015) 15976–15988. doi:10.3390/molecules200915976.

[62] H.M. Ashour, M.H. El-Wakil, M.A. Khalil, K.A. Ismail, I.M. Labouta, Synthesis of some (E)-6-[2-(furan-2-yl)ethenyl]-1,2,4-triazin-5-ones and their biological evaluation as antitumor agents, Med. Chem. Res. 22 (2013). doi:10.1007/s00044-012-0192-x.

[63] J. van Meerloo, G.J.L. Kaspers, J. Cloos, Cell Sensitivity Assays: The MTT Assay BT - Cancer Cell Culture: Methods and Protocols, in: I.A. Cree (Ed.), Humana Press, Totowa, NJ, 2011: pp. 237–245. doi:10.1007/978-1-61779-080-5_20.

[64] R. De Souza, P. Zahedi, R.M. Badame, C. Allen, M. Piquette-Miller, Chemotherapy Dosing Schedule Influences Drug Resistance Development in Ovarian Cancer, Mol. Cancer Ther. 10 (2011) 1289-1299. doi:10.1158/1535-7163.MCT-11-0058.

[65] T.-C. Chou, P. Talalay, Quantitative analysis of dose-effect relationships: the combined effects of multiple drugs or enzyme inhibitors, Adv. Enzyme Regul. 22 (1984) 27–55. doi:https://doi.org/10.1016/0065-2571(84)90007-4.

[66] T.-C. Chou, P. Talalay, Analysis of combined drug effects: a new look at a very old problem, Trends Pharmacol. Sci. 4 (1983) 450–454. doi:https://doi.org/10.1016/0165-6147(83)90490-X.

[67] U. Puapaiboon, J. Jai-nhuknan, J.A. Cowan, Characterization of a multi-functional metal-mediated nuclease by MALDI-TOF mass spectrometry, Nucleic Acids Res. 29 (2001) 3652–3656. doi:10.1093/nar/29.17.3652.

[68] Z.J. Shire, G.R. Loppnow, Molecular beacon probes for the detection of cisplatin-induced DNA damage, Anal. Bioanal. Chem. 403 (2012) 179–184. doi:10.1007/s00216-012-5790-4.

[69] A.F. El-Yazbi, G.R. Loppnow, Detecting UV-induced nucleic-acid damage, TrAC Trends Anal. Chem. 61 (2014) 83–91. doi:https://doi.org/10.1016/j.trac.2014.05.010.

[70] J.A. War, S.K. Srivastava, S.D. Srivastava, Design, synthesis and DNA-binding study of some novel morpholine linked thiazolidinone derivatives, Spectrochim. Acta Part A Mol. Biomol. Spectrosc. 173 (2017) 270–278. doi:https://doi.org/10.1016/j.saa.2016.07.054.

[71] N. Shahabadi, L. Heidari, Binding studies of the antidiabetic drug, metformin to calf thymus DNA using multispectroscopic methods, Spectrochim. Acta Part A Mol. Biomol. Spectrosc.

97 (2012) 406–410. doi:https://doi.org/10.1016/j.saa.2012.06.044.

[72] A.F. El-Yazbi, G.R. Loppnow, Terbium fluorescence as a sensitive, inexpensive probe for UV-induced damage in nucleic acids, Anal. Chim. Acta. 786 (2013) 116–123. doi:https://doi.org/10.1016/j.aca.2013.04.068.

[73] A.F. El-Yazbi, A. Wong, G.R. Loppnow, A luminescent probe of mismatched DNA hybridization: Location and number of mismatches, Anal. Chim. Acta. 994 (2017) 92–99. doi:https://doi.org/10.1016/j.aca.2017.09.036.

[74] A.F. El-Yazbi, G.R. Loppnow, Probing DNA damage induced by common antiviral agents using multiple analytical techniques, J. Pharm. Biomed. Anal. 157 (2018) 226–234. doi:https://doi.org/10.1016/j.jpba.2018.05.019.

[75] 2016. Molecular Operating Environment (MOE), Chemical Computing Group Inc.: Montreal, QC, Canada, No Title, (n.d.).

[76] J. Nekvinda, D. Różycka, S. Rykowski, E. Wyszko, A. Fedoruk-Wyszomirska, D. Gurda, M. Orlicka-Płocka, M. Giel-Pietraszuk, A. Kiliszek, W. Rypniewski, R. Bachorz, J. Wojcieszak, B. Grüner, A.B. Olejniczak, Synthesis of naphthalimide-carborane and metallacarborane conjugates: Anticancer activity, DNA binding ability, Bioorg. Chem. 94 (2020) 103432. doi:https://doi.org/10.1016/j.bioorg.2019.103432.

[77] F. Wu, L. Zhou, W. Jin, W. Yang, Y. Wang, B. Yan, W. Du, Q. Zhang, L. Zhang, Y. Guo, J. Zhang, L. Shan, T. Efferth, Anti-Proliferative and Apoptosis-Inducing Effect of Theabrownin against Non-small Cell Lung Adenocarcinoma A549 Cells , Front. Pharmacol. . 7 (2016) 465. https://www.frontiersin.org/article/10.3389/fphar.2016.00465.

Highlights

- Optimization strategy led to design and synthesis of new 1,3,5-triazinyl chalcone hybrids.
- Combination of cisplatin with the synthesized compounds resulted in significant inhibition of A549 cancer cells viability with hybrids **10** and **12**.
- Mechanism of induced DNA damage by **10** and **12** and their combination with cisplatin was studied using analytical and apoptosis induction assays.
- Molecular docking simulations were conducted to evaluate the binding mode of **10** and **12** to DNA dodecamer.
- Results confirmed the successful impact of **10** and **12** to potentiate the anticancer effect of cisplatin in A549 cells.

Graphical Abstract

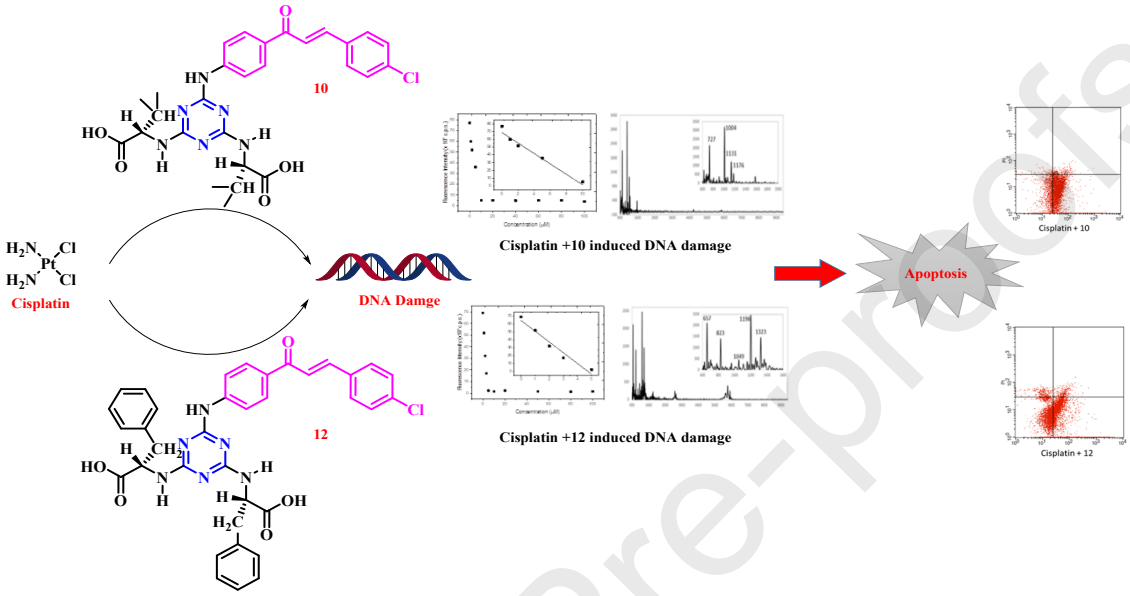

Declaration of interests

☒ The authors declare that they have no known competing financial interests or personal relationships that could have appeared to influence the work reported in this paper.

☐The authors declare the following financial interests/personal relationships which may be considered as potential competing interests: